Identification for Control of Variable Impedance Actuators

Tesi di Dottorato

Dottorato di Ricerca in:

Automatica, Robotica e Bioingegneria

Ciclo XXII (2007/8/9)

Supervisore:

Antonio Bicchi

Studente:

Giorgio Grioli

Università degli Studi di Pisa
Dipartimento di Sistemi Elettrici e Automazione

UNIVERSITÀ DI PISA

Abstract

Development of Variable Impedance Actuators (VIA) is a recent evolution in robotics to face challenges as adaptability to the environment, energy saving, safety and robustness. VIA allow to change the impedance of the limbs of a robot using physical elastic and dissipative elements rather than through traditional Impedance Control.

This leads to the problem of controlling a VIA, one important aspect of this problem lies in the absence of sensors able to measure on-line the mechanical impedance of a system. This thesis deals with the problem of impedance parameters observation in a VIA robot. This in order to develop an instrument to be used in implementing real closed-loop control of impedance of a VIA.

After an introduction to VIA and traditional impedance measurement techniques, we follow an innovative approach to derive an observer able to estimate in real-time the impedance of a VIA.

In particular three observers are presented: a non-parametric stiffness observer, a parametric stiffness observer, and an impedance observer able to estimate either non-linear time-varying stiffness, as long as linear damping and inertia coefficients. Derivation of the algorithms is shown and both simulation and experimental results are presented to support the thesis.

Foreword

This thesis is presented for the obtainment of the title of *Dottore di Ricerca* (Doctor of Philosophy) by the candidate Giorgio Grioli. It covers the main part of his studies on Variable Impedance Actuation, performed within the "E. Piaggio" Interdepartmental Research Center.

During my Ph.d. course I brought forward research in the area of Physical Human-Robot Interaction and Variable Impedance Robotics, contributing to several advancements in the design and control of a novel generation of robots. However, for the sake of coherence and focus, this thesis is organized as a monograph of one of the topics investigated in my work, which I consider most innovative and impacting.

Other result of my work led to several publications and a patent application. In particular [A1, A2][1], [A3] and [A4] report about my contribution to the state of the art of Variable Impedance Actuators, with the development and characterization of VSA-2, VSA-HD and the VSA CUBE-Bot, for which a European patent application [A5] has been filed, [A6] describes the development of the DAVID

---

[1]Awarded with the ICRA 2008 best manipulation paper.

lunar exploration rover within the "ESA Lunar Challenge" competition[2], [A7, A8] are studies on human perception and learning through haptic devices and [A9] is a study on characterization of non-linear chaotic systems.

My work is framed within two international research projects funded by the European community: PHRIENDS [W13] and VIAC-TORS [W14], both related to Physical Human-Robot Interaction and Variable Impedance Actuation.

[2]The team of the University of Pisa qualified for the final phase of the competitions and qualified on the second place.

Contents

CONTENTS

List of Figures

Acknowledgments

I would like to gratefully acknowledge all the people who aided me during these years and in the development of this thesis. In particular my family and friends, for always sustaining me in my decisions and motivating me to follow my interests, and my tutor Antonio Bicchi with all of my colleagues for giving me the opportunity to work in one of the best robotics laboratories in the world.

Introduction

Theory of impedance is of capital importance when modeling a complex mechanical system, in order to understand its behavior and to control it as well. Modeling a mechanical system through impedance is, nowadays, a very consolidate and rooted technique, and almost every engineering book is based on such approach.

Nevertheless, in the 80's, the concept of impedance has found novel application in the field of robotics, as a mean to *design* the control of a robotic manipulator which is deemed to interact with the environment. Neville Hogan proposed in [16] the so-called *Impedance Control*. He proposed the idea of designing the control law of a robot in order to let its exposed behavior be that of an impedance. Since the environment surrounding a robot can usually be modeled as an admittance, the robot should behave as an impedance in order to let the two systems *complement each other* in terms of causality.

Designing the control of a robot with this strategy has two important properties: First, impedances combine in a *linear* way, even when they are non-linear, so if the dynamic behavior of the robot is built out of a set of "Impedance blocks" the resulting impedance is just the sum of those blocks. Second, impedances are passive

mechanical systems, thus designing a controller which lets a robot behave as an impedance allows for important consideration about the stability of the overall interaction dynamics [17].

The birth of Variable Impedance Actuation

The development of robots which can operate outside a structured environment (e.g. factories) and can interact with unknown scenarios, people and even other robots, is one of the main goals of Robotics itself. Impedance control was is important instrument to face such problems.

Most of today's robots are built with rigid links and joints, thus Impedance Control is obtained through design of suitable control laws, ultimately hiding the robot with a virtual (software or active) impedance.

More recent robotic research shifted toward a new paradigm of intrinsically compliant robots. Intrinsic (hardware or passive) impedance in robots can empower many applications, for example allowing safety [18], and interaction control [16], saving energy [19], and preserving mechanisms integrity [20]. The first design solutions to take advantage of this idea consisted in the introduction of linear springs between the actuators and the links of a robot [21]. This approach was later improved by realizing actuators which integrated adjustable stiffness, where springs, which could be tuned to the particular task [22].

Latest developments led to a new category of devices, which goes under the name of Variable Stiffness Actuators or VSA, actuators with the possibility to tune stiffness during the execution of the task

INTRODUCTION

itself [23], and [24] (for a complete reference see [25]). Recently, devices which can also regulate damping [26] or inertia [27] have been proposed, thus generalizing Variable Stiffness Actuators (VSA) in Variable Impedance Actuators (VIA) This new trend aims toward the development of VIA [W14] that can adapt to the particular tasks and even during the task itself, changing the shape of their output dynamic characteristic, eventually with more than one degree of freedom of impedance adjustment.

Control of a Variable Impedance Actuator

From the most general viewpoint a Variable Impedance Actuator device is a motor that presents a certain input-output characteristic which can be changed with at least two degrees of freedom, giving the ability to regulate both the output rest position (thus the word actuator in the name) and, to a certain extent, the shape of the output characteristic (thus Variable Impedance). The presence of these two degrees of freedom in the control is what gives these devices their main advantages. Nevertheless this important feature opens an interesting problem, that is: how this second control input has to be used. This problem can be further decomposed in at least three parts (symbolically resumed in the picture):

1. How to design the impedance trajectory in order to obtain some goal,

2. how to match the actuator impedance to the desired one,

3. how to measure impedance in order to regulate it.

Problem number 1 is an optimization problem, that in the more general case, also presents constraints. While solving techniques are not always trivial and resort to numeric methods, it is more relevant to state which is the problem to be solved, i.e. the choice of the target function and the constraints. One important specialization of this problem is the safe brachistochrone, answering the question of time optimization with safety constraints; other typical approaches are energy saving or transmission, and vibration damping just to name some. Other approaches, finally, aim to the imitation of human or animal behavior patterns.

Question number 2 translates in the control problem of a, typically, non-linear system. It can be solved using classical control theory: PD regulator and feedback linearization are just two of the solutions that were presented in literature.

The third problem is, in the opinion of the author, the one still offering the largest improvement margins, and is the main topic of this thesis. The typical solution, which has been almost universally adopted in literature, is to measure the internal configuration of the VIA device and, through a model of it, reconstruct what the actual Impedance value is. This approach to the problem presents all the typical drawbacks imputable to model-based control: heavy reliance on the knowledge of the model brings arbitrary sensitivity to errors in model and parameters.

The new research line, that has been followed in this work, is the design of an algorithm to observe Impedance, which, relying on the few prior knowledge as possible, is able to estimate in real-time the value of the output impedance. This in order to feed it to the regulator and, eventually, to the higher level in the control and planning

INTRODUCTION

hierarchy, implementing real closed loop control of impedance in a VIA.

Executive Summary

First chapter is an introduction to the concept of impedance of a mechanical system, from its intrinsic differential nature to the various elements that physically constitute impedance.

Second chapter presents and discusses some commercial and academic techniques to identify the impedance of mechanical systems, derived from the fields of vibration theory, biophysics and robotics.

Chapters three, four and five, finally, presents the main results consisting in the derivation of a method for the on-line identification of the impedance of a VIA robot.

In particular, chapter three presents a non-parametric method for the identification of the non-linear time-varying stiffness of a Variable Stiffness Actuator (VSA, a particular kind of VIA).

Chapter four extends results of chapter four with a parametric stiffness observer, showing how its performance can overcome some limitations of the non-parametric observer.

Finally, chapter five extends the framework to allow also the estimation of the inertial and damping components of the impedance.

Chapter 1

An introduction to Impedance
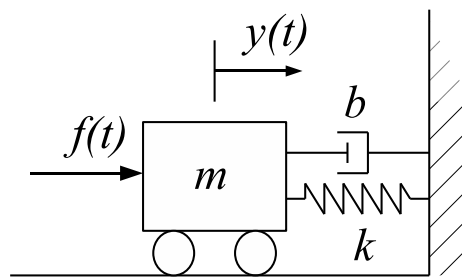
Figure 1.1: A simple mass-spring-damper system.

The concept of impedance in mechanics is borrowed from the field of circuit theory: electric impedance measures how strongly a circuit or component opposes to the transit of current through it with the generation of a voltage at its extremes. In analogy, me-

chanical impedance is the measure of how much a body or structure resists to motion or deformation with the generation of a force (or torque). To introduce impedance in a more formal way, consider the paradigmatic example of a mass-spring-damper system (see fig. 1.1), described as a relation between the applied force $f(t)$ and displacement $y(t)$ through

$$f = m\ddot{y} + b\dot{y} + ky. \tag{1.1}$$

the three parameters m, b, k are constant, the O.D.E. (1.1) is linear and time-invariant. Introducing the Laplace transforms $F(s), Y(s)$ of force and position, one has immediately

$$F(s) = (ms^2 + bs + k)Y(s). \tag{1.2}$$

The operator $Z(s) := (ms^2 + bs + k)$ is called the *mechanical impedance* of the spring-damper-mass system[1]. The reciprocal operator of impedance, called *admittance* (or *mobility*) $A(s)$, generalizes compliance as it maps forces in displacements: $Y(s) = A(s)F(s)$. The admittance operator is causal, while impedance is not.

---

[1]It should be noted that in the literature, the term *impedance* is sometimes used to denote the relationship between velocity and force, maintaining a stricter adherence to the electrical metaphor.

1.1 Variational approach

The above approach can be generalized to a nonlinear dynamic setting by considering the relation between forces, displacements, first and second derivatives of displacements, and internal states u, and its graph $G \subset F \times Y \times DY \times D^2Y \times U$, comprised of 5-tuples $d(t) := (f(t), y(t), \dot{y}(t), \ddot{y}(t), u)$ corresponding to an idealized, infinite set of experiments. If $G(f, y, \dot{y}, \ddot{y}, u) = 0$ is an analytical description of the graph, and d_0 is a regular point, then a *force function* $f(y, \dot{y}, \ddot{y}, u)$ is defined in a neighborhood of d_0. Defining *generalized stiffness* as

$$k(d) = -\left(\frac{\partial G(d)}{\partial f} \right)^{-1} \frac{\partial G(d)}{\partial y}, \qquad (1.3)$$

generalized damping as

$$b(d) = -\left(\frac{\partial G(d)}{\partial f} \right)^{-1} \frac{\partial G(d)}{\partial \dot{y}}, \qquad (1.4)$$

generalized mass as

$$m(d) = -\left(\frac{\partial G(d)}{\partial f} \right)^{-1} \frac{\partial G(d)}{\partial \ddot{y}}, \qquad (1.5)$$

and *generalized I/O trans-characteristic* as

$$\nu(d) = -\left(\frac{\partial G(d)}{\partial f} \right)^{-1} \frac{\partial G(d)}{\partial u}, \qquad (1.6)$$

one can compute the Frèchet differential of the force function as

$$\delta f = m(d)\, \delta\ddot{y} + b(d)\, \delta\dot{y} + k(d)\, \delta y + \nu(d)\, \delta u \ . \qquad (1.7)$$

From consideration of the positive definiteness of the kinetic energy, the Rayleigh dissipation function, and the elastic energy associated

with the generalized inertia, damping and stiffness, it follows that m, b, and k are always greater than zero (or positive definite).

Alternatively, one can describe admittance along a given trajectory as the linear operator mapping small changes of the external force to changes in the resulting motion. To do this, consider the nonlinear ODE obtained by solving $G(f, y, \dot{y}, \ddot{y}, u, t) = 0$ at a regular point with respect to $\ddot{y}$ as

$$\ddot{y} = g(y, \dot{y}, f, u)$$

and its state space form, with $x \in \mathbb{R}^2$, $x_1 = y$, $x_2 = \dot{y}$, i.e.

$$\frac{d}{dt} \begin{bmatrix} x_1 \\ x_2 \end{bmatrix} = \begin{bmatrix} x_2 \\ g(x_1, x_2, f, u) \end{bmatrix}$$

For given initial conditions $x(0) = \bar{x}_0$ and a given course in time for force $\bar{f}(t)$ and input $\bar{u}(t)$, let $\bar{x}(t)$ be the trajectory obtained, i.e. the solution of the dynamics ODE. The first-order approximation of the dynamics of the perturbed motion $\tilde{x}(t) = x(t) - \bar{x}(t)$ corresponding to a change in force $\tilde{f}(t) = f(t) - \bar{f}(t)$ is the time-varying linear system

$$\dot{\tilde{x}} = \Gamma(t)\tilde{x} + \Theta(t) \begin{bmatrix} \tilde{f} \\ \tilde{u} \end{bmatrix},$$

where

$$\Gamma(t) = \begin{bmatrix} 0 & 1 \\ -\frac{k(d)}{m(d)} & -\frac{b(d)}{m(d)} \end{bmatrix}, \Theta(t) = \begin{bmatrix} 0 & 0 \\ \frac{1}{m(d)} & \frac{\nu(d)}{m(d)} \end{bmatrix}.$$

1.2 Impedance Components

This section pans over the various elements contributing to the impedance of a mechanical system.

1.2.1 Stiffness

(a) traction   (b) compression   (c) torsion
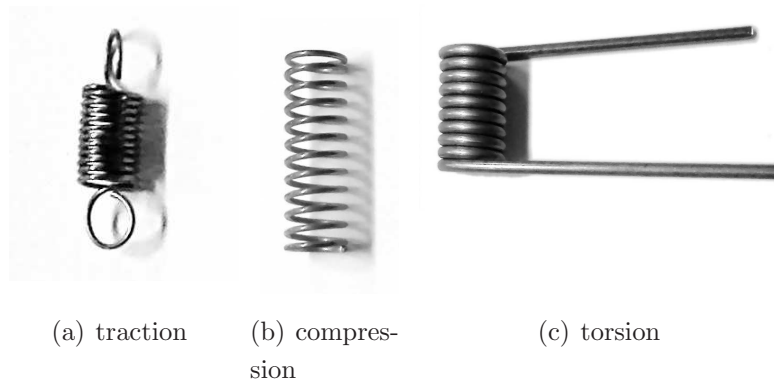
Figure 1.2: Typical linear springs.

The simplest example of mechanical impedance is a *spring*, i.e. a sample of material characterized by the property of *elasticity*. This property consists in the fact that the body exerts a force when deformed. In an ideal spring the relation between the applied force f and the steady–state displacement y can be expressed as a function:

$$f = f(y). \tag{1.8}$$

An important parameter used to characterize a spring is the derivative of the force f with respect to the deformation y:

$$\sigma(y) \triangleq \frac{\partial f(y)}{\partial(y)}, \tag{1.9}$$

this quantity is defined as *spring rate* or *stiffness* of the spring. In linear springs

$$f(y) = ky, \qquad (1.10)$$

thus the constant k is the spring stiffness. The relation expressed in 1.10 was first devised by the English scientist Robert Hooke[2] in 1660 [28], from whom takes the name of *Hooke Law*.

In general, the force function of real springs $f(y)$ can be nonlinear and time-varying. Its behavior may depend on a vector of parameters u (which represent internal states and/or, as it is the case of VIA, inputs), which in turn may vary in time. Stiffness σ is, in this more general case, defined as

$$\sigma(y, u) \triangleq \frac{\partial f(y, u)}{\partial y}. \qquad (1.11)$$
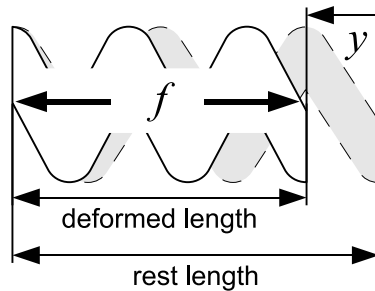
Figure 1.3: Schematic diagram of a deformed spring.

In some texts the definition of stiffness differs from that presented in equations 1.9 and 1.11 by the introduction of a minus sign. The

[2]Robert Hooke, 18 July 1635 – 3 March 1703, was an English natural philosopher, architect and polymath, who played an important role in the scientific revolution.

1.2 Impedance Components

apparent confusion arises only from the adoption of different reference systems for the definition of f and y. To clarify this, refer to figure 1.3, so to follow the rule that stiffness is *positive* when it is such that the spring exerts a recoil force, so to *oppose to the deformation*.

1.2.2 Inertia

Figure 1.4: Sample reference masses used for weighting. Mass is the cause of inertial forces.

Inertia is the property of a body to oppose to a change in its status of rest or motion with a force. The classical concept of inertia goes back to the very foundations of classical mechanics, with the principle of inertia, discovered by Galileo[3] and described by Newton[4] in its *Principia* [29]. Notwithstanding its long history it is still, among physicists, a debuted and not fully eviscerated concept, rooting in the fields of relativity and quantum physics.

---

[3]Galileo Galilei, 15 February 1564 – 8 January 1642, was an Italian physicist, mathematician, astronomer and philosopher who played a major role in the Scientific Revolution.

[4]Sir Isaac Newton, 4 January 1643 – 31 March 1727, was an English physicist, mathematician, astronomer, natural philosopher, alchemist, and theologian. His "PhilosophiæNaturalis Principia Mathematica", [29], published in 1687, lays the groundwork for most of classical mechanics.

1.2 Impedance Components

Limiting our analysis to 'relativistically slow' and 'quantically big' mechanical systems, Newton's definition of inertia (from [29]) is valid:

> The vis insita, or innate force of matter, is a power of resisting by which every body, as much as in it lies, endeavours to preserve its present state, whether it be of rest or of moving uniformly forward in a straight line.

The most important aspect about inertia is that a body characterized by inertia I and moving with velocity v can be associated with a momentum p and a kinetic energy T, defined as

$$p \triangleq Iv \tag{1.12}$$

$$T \triangleq \frac{1}{2}v^T Iv. \tag{1.13}$$

Velocity and momentum are scalars for motions along one degree of freedom (e.g. linear motion, where the inertia corresponds to the mass of the body) but can be generalized to vectors (e.g. for spatial motions of a rigid body) and in such cases inertia is a square matrix (the inertia tensor).

The last important effect of inertia is described by the second law of classical dynamics yielding that whenever there is a change in the generalized momentum p (associated with an inertia I) it can be related to the generalized force generating it by

$$f \triangleq \frac{dp}{dt} = I\dot{v} + \dot{I}v, \tag{1.14}$$

where the inertial force is due to both the change in velocity (acceleration) and the rate of change of the inertia matrix.

As for stiffness, inertia can be non-linear and time-varying, as is the case for the inertia matrix $M(q)$ of a robot, which is a function of its joint configuration vector q.

1.2 Impedance Components

1.2.3 Damping

Figure 1.5: A damper used for car suspensions.

Damping is a property of some mechanical bodies to dissipate kinetic energy, transferring it into the thermal domain. There can be many sources of dissipation in a mechanical system, which most of the times can be ultimately reduced to frictions phenomena. In classical mechanics, the assumption of the existence of *damping elements*, or *dampers*, can be made: they are bodies that oppose to deformation y a force f (in this similar somehow to springs) which is a function of the deformation rate $\dot{y}$, as:

$$f = f(\dot{y}). \tag{1.15}$$

In analogy to springs, the parameter *damping* can be defined, which is the partial derivative of the force with respect to the deformation rate:

$$\delta = \frac{\partial f}{\partial \dot{y}}. \tag{1.16}$$

The simplest example of damper is, the linear viscous damper,

which models the phenomenon of viscous friction, where

$$f = b\dot{y}. \tag{1.17}$$

Another common but non-linear example is dynamic friction, for which it holds

$$f = b\,\mathrm{sign}(\dot{y}). \tag{1.18}$$

1.2 Impedance Components

1.2.4   Transmission ratio

Figure 1.6: A pair of gears used for transmission of motion.

The last fundamental "brick" of impedance left to be considered is transmission ratio. It is not, strictly speaking, an impedance, but rather a trans-impedance, which describes the interaction of two bodies. It arises from a constraint between two elements of a system binding the generalized displacement of one element to that of the other. This generates, dually, an algebraic relationship also between the generalized forces transmitted through the two elements. Given the two generalized coordinates y_1 and y_2 for the two bodies, and the two associated generalized forces f_1 and f_2, the existence of a transmission ratio between the two bodies can be specified as a relation among the speeds and the forces of the two bodies as:

$$\begin{cases} \dot{y}_1 & = & r(y_1, y_2, u)\dot{y}_2 \\ f_2 & = & r(y_1, y_2, u)f_1, \end{cases} \qquad (1.19)$$

where the u accounts for eventual variability of the ratio itself.

The second equation of 1.19 is a straight consequence of the fact that a transmission ratio is the effect of a constraint, thus, at ev-

ery instant, it does not absorb nor produce energy. Applying the principle of virtual works yields the result.

Many kinds of transmission ratios, associated with the many possible mechanical couplings, exist, linking two or more mechanical elements. One of the simplest examples is a spur-gear pair, as in figure 1.6. For such a system the transmission ratio is a fixed constant r, derived from the ratio of teeth in the two gears, thus it yields

$$\begin{cases} \dot{y}_1 & = & r\dot{y}_2 \\ f_2 & = & rf_1, \end{cases} \tag{1.20}$$

Another common example is the shift gearbox used in automobiles, where $r = r(u)$ and $u \in \{1, 2, 3, 4, 5, R\}$. It can be noticed how this system is linear but time-varying.

Another example worthwhile mentioning is the Jacobian matrix of a serial robot, which is a multi-dimensional generalization of the concept of transmission ratio, expressing the relationship between the speed of the joints $\dot{q}$ and the speed of the end-effector $\dot{x}_{EE}$ as a function of the joints coordinates q, as

$$\dot{x}_{EE} = J(q)\dot{q}, \tag{1.21}$$

the dual relationship maps forces acting on the end effectors f_{EE} on the torques felt at the joint levels as

$$\tau = J^T(q)f_{EE}. \tag{1.22}$$

1.3   Model of a Variable Impedance Actuator

Given all the previous definitions, it is possible to define a little more in detail what a Variable Impedance Actuator is. Assume, for
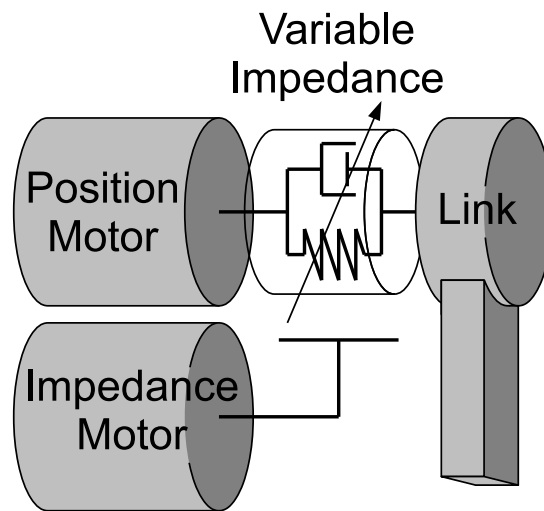
Figure 1.7: Schematic of a generic Variable Impedance Actuator. Position Motor indirectly moves the Link trough the Variable Impedance element actuated by Impedance Motor.

sake of simplicity, a VIA mechanism characterized by 3 degrees of freedom (DOFs) as is the case for most of the prototypes developed nowadays. Without loosing much detail a VIA can be modeled as one motor (indirectly) actuating the link movement and another motor actuating the impedance variation, as in Fig. 1.7, or:

$$\begin{cases} I\ddot{q} + N\dot{q} + F(\theta_2, \cdots) = \tau_{ext} \\ B_1\ddot{\theta}_1 + D_1\dot{\theta}_1 - F(\theta_2, \cdots) = \tau_1 \\ B_2\ddot{\theta}_2 + D_2\dot{\theta}_2 + G(\theta_2, \cdots) = \tau_2. \end{cases} \qquad (1.23)$$

The first equation of 1.23 represents the dynamics of the link: I, N and $\Sigma(\theta_2, \cdots)$ are inertia, damping and the non-linear variable impedance of the link, respectively, τ_{ext} is the external torque on the link, q is the link angle. The second equation of 1.23 represents the dynamics of the position actuating motor: B_1 and D_1 are inertia and damping of the link motor, respectively, τ_1 is the motor torque and θ_1 is the motor angle. The third equation represents the dynamics of the impedance actuating motor: B_2 and D_2 are inertia and damping of the stiffness motor, respectively. $G(\theta_2, \cdots)$ is the torque needed for the motors to change impedance and τ_2 and θ_2 are the motor torque and angle, respectively.

The functions

$$\begin{aligned} F(\theta_2, \cdots) &= F(\theta_2, q - \theta_1, \dot{q} - \dot{\theta}_1, \ddot{q} - \ddot{\theta}_1, \cdots) & (1.24) \\ G(\theta_2, \cdots) &= G(\theta_2, q - \theta_1, \dot{q} - \dot{\theta}_1, \ddot{q} - \ddot{\theta}_1, \cdots) & (1.25) \\ &, & (1.26) \end{aligned}$$

represent the *variable impedance* part of the system. Their effective structure and the set of their arguments depend on the particular VIA system considered. It can usually be restricted to the values of θ_2, $q - \theta_1$ and their derivatives. In the case of a VSA, i.e. a VIA where damping and inertia are constant, the arguments of $F()$ and $G()$ reduce to just θ_2, $q - \theta_1$, respectively.

Chapter 2

Impedance measuring techniques

2.1 Metrology and Instrumentation

Adopting the definitions of section 1 follows that impedance is a differential operator relating two physical quantities and not a physical quantity *per se.* Here the definition of physical quantity given in [30] is adopted:

> Physical quantity - a property of a phenomenon, body, or substance, where the property has a magnitude that can be expressed as a number and a reference.

As a consequence of this, the characterization of the impedance of a mechanical system is not a direct measurement, but instead it is performed as a process of identification of a dynamical system (see for example [31]).

Breaking down impedance of a system in its fundamental components, direct measurements are sometimes possible (e.g. measuring a the mass of a body), nevertheless, such measurements are not, in general, possible.

Moreover, the possibility to directly measure impedance components is sometimes unpractical or unfeasible; this happens, for example, when the considered component of impedanceis non-linear (e.g. the mechanical characteristic of a non-linear spring). In this case one has to resort to the acquisition of a set of force and displacement data pairs (or their derivatives).

After this step, if a theoretic model of the spring is available, parametric fitting techniques can be adopted to extract from the dataset a reconstruction of the underlying non-linear function. Otherwise numerical derivation technique must be employed to resort to the spring stiffness.

The first devices to characterize the impedance of a mechanical systems were proposed in the 40's of 20th century, (see for example [32] and [33]). Their evolution led to the creation of the so-called "impedance head", which is discussed in the next section.

2.1 Metrology and Instrumentation

2.1.1 Impedance Heads
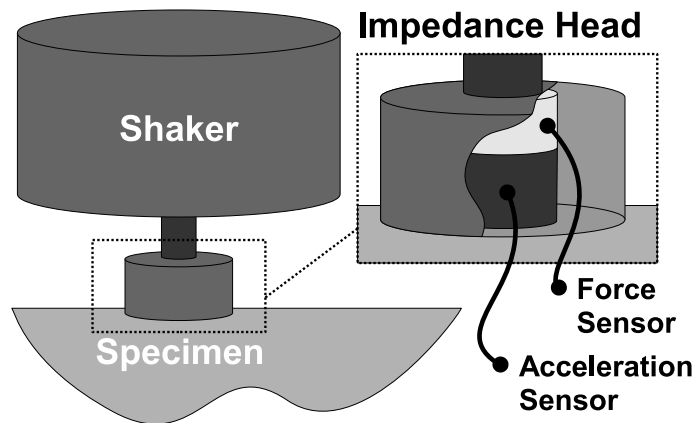
Figure 2.1: Typical set-up for the characterization of mechanical impedance.

The most common technique for the characterization of mechanical impedance relies the the application of a forced vibration on the specimen and the simultaneous recording of the applied force and the resulting acceleration (as in figure 2.1).

To successfully achieve simultaneous acquisition of both force and acceleration measurements, a particular kind of sensor is adopted, which goes under the name of impedance head (an example is shown in figure 2.2). It consists, substantially, in the combination of a load cell and an accelerometer (both realized with piezoelectric technology in modern devices), assembled such that the acceleration sensor can be firmly attached to the specimen.

Exact procedures for the acquisition of the data may vary de-

Figure 2.2: Picture of a commercial impedance head. Positioning labels can be noticed to help correct mounting of the sensor on the specimen. Image from [W15].

pending on the advices of the particular impedance head, and the material of the specimen. Detailed procedure descriptions are available in specific literature, as [31].

The straightforward application of such technology to VIA robot systems is possible just during off-line calibration and identification, requiring usually for the VIA to be disassembled from the robot.

2.2 Impedance measurement on biological systems

A field where joint impedance measurement has already received wide attention is Biophysics. Techniques for measuring the stiffness of the human limbs have been proposed over the years. The biggest problem arising when experimenting with biological systems, consists in the difficulty to separate the different simultaneous phenomena contributing to some effect. Limb impedance is not an exception.

Two major approaches can be followed to overcome this obstacle, namely invasive and non-invasive. Invasive investigation techniques will not be discussed in depth here, just remember that, on biological system, they can range from acquisition of both live and dead samples, to study on test animals/subjects.

While such "drastic" techniques can help to understand the intrinsic properties of biologic tissues constituting the musculo-skeletal system, non-invasive techniques are, on the other hand, important and necessary. Their application, indeed, allows studying the behavior of live systems as a whole, and lead to insight of the global system as well as to the development of diagnostic tools which can be used by physicians.

For a deeper introduction to the topic of impedance measurement in bio-engineering refer to [34] or [35]. The main claim here is that most methods address very specific tasks within very well determined experimental condition. Such tasks are often very static.

To the best knowledge of the author, all the non-invasive methods adopted in bio-engineering and physiology literature to measure

impedance resort to a model of the system whose impedance is going to be measured. They identify the parameters of that model, and modeling muscles is still a controversial matter.

One of the few examples of dynamic setup for limb impedance identification is the one proposed by [36]. The proposed method identifies stiffness based on the outcome of a series of repeated execution of a trajectory by the subject. A first a set of the repetitions is used to infer the reference motion of the limb. Thereafter, the next set is used to inject disturbances and measure the reaction forces. Stiffness is then calculated fitting the amplitude of recorded forces and injected disturbances to a linear model.

This method is designed in this way to circumvent two problems. The first one lies in the impossibility to know the reference position with respect to which the stiffness is defined. This is due to the intrinsic non-invasiveness of the procedure and to the lack of knowledge of precise muscle models. To understand the effect of ignoring the limb reference on the identification of its impedance, just look at figure 2.3. Using the y_h (where the subscript h stands for halfway) as reference instead of y_0 yields a spring which deforms half the amount of the full one, thus with double the stiffness. This phenomenon can not be easily circumvented due to the fact that it is not an error on the method but rather an intrinsic ambiguity on the frame with respect to which impedance is defined.

The second obstacle to overcome is separation of the passive and active responses of the subject. Here passive response is used to intend the response due to the effective stiffness of the musculo-skeletal system, while active response encompasses all the effect which involve nervous system, as reflexes and conscious reactions.

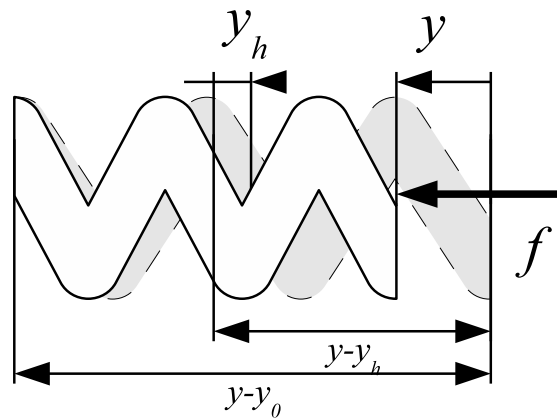## 2.2 Impedance measurement on biological systems

Figure 2.3: Effect of wrong reference trajectory in the estimation of stiffness. If the deformation is measured with respect to the wrong reference frame (y_h in the image), the error on estimation of stiffness can be substantial, altering completely the relationship between the force and the yielding deformation. Given the spring in figure is linear with stiffness K, an observer measuring deflection with respect to y_h instead of y_0 would measure a stiffness of $2K$. Note that this, rather than being an error is a pure matter of observation relativity: the "half spring" comprised between y_h and y has, indeed, double stiffness with respect to the full spring.

Overcoming this second problem is usually possible performing the measurement during the short time that starts on the instant when the perturbation is applied and lasts when the first active response arises. This time is well measured in humans and lasts around 100 ms, due to the travel time of the nervous pulses from the senses to the spinal chord and back to the muscles.

Impedance identification methods proposed for biological systems are a step nigher to on-line identification of impedance of VIA robots, but still do not apply to our case due to the high specificity of their models and the requirement of injecting controlled perturbations on the system.

2.3 Impedance Estimation in Robotics

Within robotics literature, some attention has been dedicated to the problem of impedance identification for tasks that involve contact between the robot and the external world. In this case the impedance being identified is that of the environment. This allows for a more effective and controlled manipulation of the environment itself by the robot. For example [37] suggests the estimation of impedance to improve effectiveness of food processing; the estimation of impedance is obtained, in this work, through estimation of contact forces and measurement of contact point speed, which the author suggest to feed to a digital Kalman filter [38] designed on a model of linear impedance.

In [39] estimation of contact impedance is proposed as a mean to improve tasks such as telemanipulation. There the authors stress the importance of adopting a non-linear Hunt-Crossley model [40] rather than the simpler linear Kelvin-Voight model. Thereafter a recursive least square technique is adopted to build an *ad-hoc* observer to successfully estimate the parameters of the model.

Work [41] is a nice review on four different techniques proposed for the estimation of contact stiffness and damping in robotic contact problems, namely: *Signal Processing Method*, *Indirect Adaptive Control*, *Model Reference Adaptive Control* and *Recursive Least Squares*. All of the proposed approaches are shown to be capable of estimating the parameters of the contact model (which is always *linear*), if conditions of *persistent excitation* are met, otherwise some estimation is still possible to some extent, depending on the observer gains and the particular maneuver of the robot contacting the environment.

Recent works propose more sophisticate algorithms for contact stiffness identification, like [42], or specialize their approaches for particular types of sensors, like [43], or take into account the effects on non-ideality of the model on the estimation process, as [44].

The various approaches followed by all the previous works have in common reliance on the knowledge of the the model of the impedance to be estimate (which is most often assumed linear).

These works are the nearest to the method that this thesis is are going to develop in the next chapters.

Chapter 3

Non-parametric identification of stiffness

This and the next two chapters contain the major contribution of this thesis. Results exposed in chapters 3, 4 and 5 are published in [A10], [A11] and [A12], respectively.

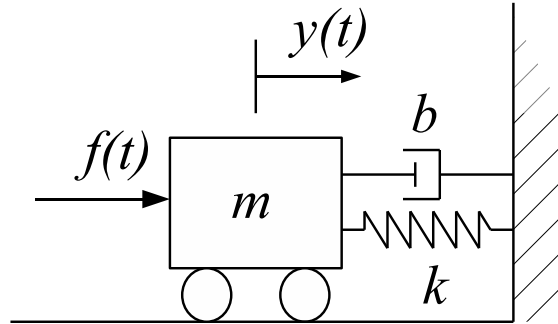## 3.1 Impedance observability in a linear mechanical system

Figure 3.1: A simple linear mass-spring-damper system.

Resorting to the system of figure 1.1, it can be described by equation 1.1, as

$$m\ddot{y} + b\dot{y} + ky = f \qquad (1.1)$$

consider the extended state vector $z = \begin{bmatrix} y & \dot{y} & -\frac{k}{m} & -\frac{b}{m} & \frac{1}{m} \end{bmatrix}$, the dynamics of 1.1 can be and rewritten as

$$
\begin{aligned}
\dot{z} &= \begin{bmatrix} z_2 \\ z_1 z_3 + z_2 z_4 \\ 0 \\ 0 \\ 0 \end{bmatrix} + \begin{bmatrix} 0 \\ z_5 \\ 0 \\ 0 \\ 0 \end{bmatrix} f, \\
y &= h(z) = z_1.
\end{aligned}
\qquad (3.1)
$$

The identification of the impedance parameters can thus be cast as a nonlinear state estimation problem, i.e., from the measurement of the

3.1 Impedance observability in a linear mechanical system

external force f and position y, estimate the initial state $z(0)$, and in particular its three last components which completely determine the linear impedance.

To establish that the problem is well posed, consider the observability codistribution for this system,

$$
\Omega(z) = \begin{bmatrix}
1 & 0 & 0 & 0 & 0 \\
0 & 1 & 0 & 0 & 0 \\
z_3 & z_4 & z_1 & z_2 & 0 \\
0 & 0 & 0 & 0 & 1 \\
z_3 z_4 & z_3 + z_4^2 & z_2 + z_1 z_4 & z_1 z_3 + 2 z_2 z_4 & 0 \\
0 & 0 & 0 & z_5 & z_4
\end{bmatrix}.
$$

it turns out that for $m, b, k > 0$, $\dim\Omega(z)^{\perp} = 0$, $\forall z$ except $z_1 = z_2 = 0$. Hence, if the system moves from the equilibrium, the three linear impedance parameters can be reconstructed from position and force measurements.

3.2 Impedance observability in a non-linear mechanical system

Consider now a simple mechanical system, similar to the previous one, with the only difference that the mechanical characteristic of the spring is not linear but rather a generic non-linear function, i.e.

$$f_e = f_e(y) \neq ky. \qquad (3.2)$$

Equation 1.1 transforms in

$$m\ddot{y} + b\dot{y} + f_e(y) = f. \qquad (3.3)$$

To proceed along the same steps as before, there is the need for a model of the stiffness function $f_e(y)$. If one is available, as

$$f_e(y) = f_e(p, y)$$

where p is a vector of unknown parameters of length n_p, an augmented state space can always be written as

$$z = \begin{bmatrix} y \\ \dot{y} \\ \frac{1}{m} \\ \frac{b}{m} \\ p_1 \\ \vdots \\ p_{n_p} \end{bmatrix}. \qquad (3.4)$$

3.2 Impedance obs. in a non-linear mechanical system

This state space would have dimension equal to n_p+4. The dynamics of the system can be rewritten as

$$
\dot{z} = \begin{bmatrix} z_2 \\ z_2 z_4 + z_3 f_e([z_5, \cdots, z_{n_p+4}], z_1) \\ 0 \\ 0 \\ \vdots \\ 0 \end{bmatrix} + \begin{bmatrix} 0 \\ z_5 \\ 0 \\ 0 \\ \vdots \\ 0 \end{bmatrix} f, \tag{3.5}
$$

$$
y = h(z) = z_1.
$$

To conclude on the observability of the system, one has to specify the structure of the function $f_e(p,y)$ and proceed with the calculation of the particular observability codistribution Ω, without leaving the possibility to draw generic conclusions.

The same approach can be taken also for systems where the non-linear part of the impedance is damping and/or inertia and if the system is time-varying. Again it would lead to open conclusions. Pushed by this, in the next section the problem will be faced following a slightly unconventional approach.

Now a different approach to measure stiffness in a system such as (3.3) will be described. For simplicity's sake, assume for the time being that accurate measures of the applied force $f(t)$ and of the position $y(t)$ are available, and that numerical derivatives of these signals can be done. Assume also that both the mass and damping coefficients, m and b, are known (these strong assumptions will be discussed later on). No assumptions are made on the function $f(y,u)$ except that it is smooth in both arguments, with bounded derivatives of all orders.

Assume that the stiffness-regulating input $u(t)$ is bounded with its first derivative $\dot{u}(t)$[1]. It should be noticed that, in building an observer that relies only on measurements of the position $y(t)$ corresponding to the external load $f(t)$, it is physically impossible to observe a stiffness which is changing in time $(\dot{u}(t) \neq 0)$ while the system is at equilibrium $(\dot{y}(t) = 0)$. More precisely then, the assumption that the ratio between the stiffness regulation rate of change and the velocity of the measured trajectory is bounded will be made, namely, for all times t during the application of the observer, it holds

$$\frac{|\dot{u}(t)|}{|\dot{y}(t)|} < v \in \mathbb{R}, \quad \forall t.$$

Let

$$\frac{\partial f}{\partial y} = \frac{\partial f(y, u)}{\partial y} := \sigma(y, u(t))$$

denote the stiffness to be measured. Also let $\hat{\sigma}(t)$ denote its estimate at time t, and $\tilde{\sigma}(t) = \sigma(y, u(t)) - \hat{\sigma}(t)$ be the estimation error.

Differentiate (3.3) once with respect to time to get

$$\dot{f} = m\dddot{y} + b\ddot{y} + \sigma\dot{y} + s_u\dot{u},$$

where $s_u := \frac{\partial s(y,u)}{\partial u}$. Using the current estimate of stiffness and the assumptions stated above, a best-effort prediction for $\dot{f}$ can be written (in the absence of information on $s(y, u)$ and on $u(t)$) as

$$\hat{\dot{f}} = m\dddot{y} + b\ddot{y} + \hat{\sigma}\dot{y}$$

The update law

$$\dot{\hat{\sigma}} = \alpha\tilde{\dot{f}}\mathrm{sgn}(\dot{y}), \tag{3.6}$$

---

[1]Recalling eq. 1.23, it can be proved that this is a straightforward consequence of the finiteness of the dynamic of $u = \theta_2$.

3.2 Impedance obs. in a non-linear mechanical system

with $\alpha > 0$ and

$$\mathrm{sgn}(x) := \begin{cases} \frac{x}{\|x\|} & \text{if } \|x\| \neq 0 \\[2mm] 0 & \text{if } \|x\| = 0 \end{cases},$$

can be shown to guarantee that $\hat{\sigma}(t)$ can be made to converge to the true stiffness value $\sigma(t)$ within an uniformly ultimately bounded error.

Indeed, consider the positive definite error function

$$V_\sigma := \frac{1}{2}\tilde{\sigma}^2$$

and its derivative along the trajectory defined in (3.6), i.e.

$$\dot{V}_\sigma = \tilde{\sigma}\dot{\tilde{\sigma}} = \tilde{\sigma}\dot{\sigma} - \tilde{\sigma}\dot{\hat{\sigma}} = \tilde{\sigma}\dot{\sigma} - \alpha\tilde{\sigma}s_u\,\dot{u}\,\mathrm{sgn}(\dot{y}) - \alpha\tilde{\sigma}^2|\dot{y}| \ . \qquad (3.7)$$

While the first two terms in the rightmost sum in (3.7) are indefinite in sign, the third term is negative definite. Therefore, wherever the inequality holds

$$|\tilde{\sigma}| > |s_u|\frac{|\dot{u}|}{|\dot{y}|} + \frac{1}{\alpha}\frac{|\dot{\sigma}|}{|\dot{y}|} \qquad (3.8)$$

the derivative of the error function $\dot{V}_\sigma$ is negative, hence the estimation error decreases. By writing $\dot{\sigma} = \sigma_y\dot{y} + \sigma_u\dot{u}$, and using the upper bound above assumed on the rate of stiffness change, stiffness estimates converge to the true value within an ultimately uniformly bounded error given by

$$|\tilde{\sigma}| > \frac{|\sigma_y|}{\alpha} + \left(|s_u| + \frac{|\sigma_u|}{\alpha}\right)v \qquad (3.9)$$

Remark 1 *The assumption that the mass and damping are exactly known is not realistic. However, it is easy to verify that the analysis above carries over exactly even with no knowledge of m and b, provided that a force sensor directly placed on the elastic element provides a measure of the force $f(x, u)$. In case this is not available, then errors on the m and b parameters have the effect of making the ultimate error larger (this effect can be countered by increasing the observer gain α).*

3.3 Simulation Results

As a first illustration, the proposed stiffness observer is tested using numeric simulations in two systems.

3.3.1 Single spring

In this first test, the observer algorithm is used to track the stiffness value of a single spring with non-linear, time-invariant stiffness characteristic. The simulated elastic element is an exponential spring, whose force/displacement characteristic is

$$s(y) = ae^{by} . \tag{3.10}$$

Such springs are designed so that the stiffness at any operating point is proportional to the force the spring is exchanging with the external environment.

Figure 3.2(a) compares the observer estimate of the spring stiffness with its exact value $\sigma(y) = bae^{by}$, for three different values of the spring parameters. The springs were subject to a external force
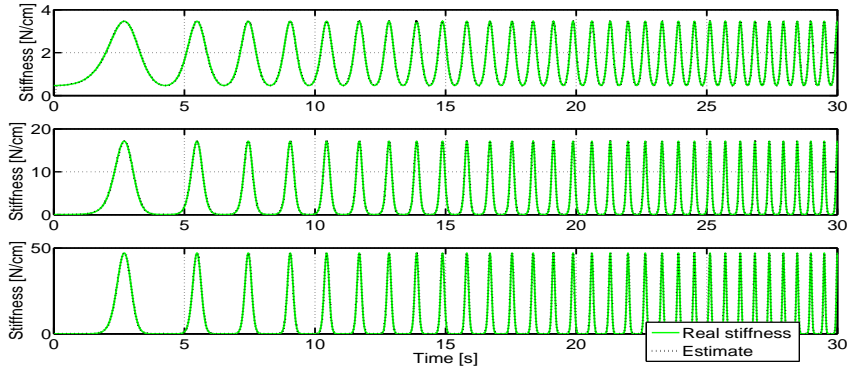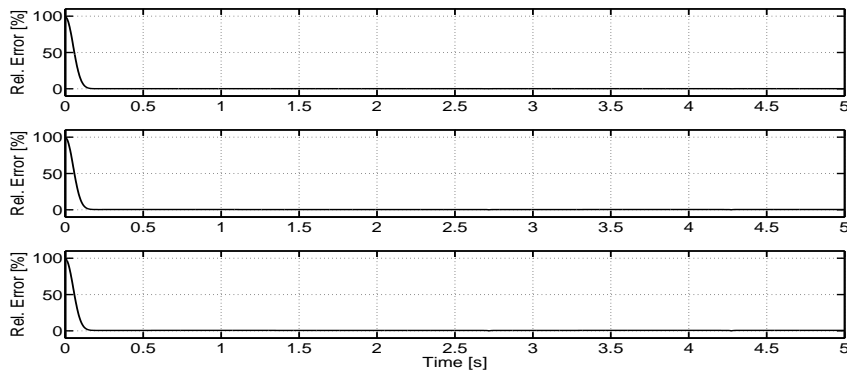
3.3 Simulation Results

$f(t)$ given by a chirp in the frequency range from 0.1 to 10 Hz, with deformations $y(t)$ in the range $[0.25, 2.25]$cm. The observation error (shown in fig. 3.2(b)) decays to less than one percent in less than 0.3 s.

(a) tracking

(b) error

Figure 3.2: Simulation results for the non-parametric observer estimating three different springs ($a = 2.7e^{-2}$, $b = 1$; $a = 8.1e^{-6}$, $b = 3$; $a = 13.5e^{-10}$, $b = 5$, respectively). Stiffness tracking is shown in panel (a), and relative estimation error in panel (b). Only the first 5s of the relative error are shown, to focus on the transient phase. Relative error remains under 1% for the rest of the time.

3.3 Simulation Results

3.3.2 Muscle-like antagonistic VSA systems

Consider the link in fig. 3.3, actuated by two antagonistic actuators (with a role vaguely similar to that of the biceps and triceps muscles at the elbow), with a quadratic damping and subject to gravity and to an external torque load τ_e. The system dynamics are

$$I\ddot{\theta} + \beta\dot{\theta}|\dot{\theta}| - \tau_b + \tau_t - mgl\sin\theta - \tau_e = 0$$

Assume first that the two actuators generate torques according to the model (cf. [45])

$$\begin{aligned} \tau_b &= (\tau_{max} - \alpha\theta_b)\, u_b \\ \tau_t &= (\tau_{max} - \alpha\theta_t)\, u_t \end{aligned} \qquad (3.11)$$

where $\theta_b = (\pi/2 + \theta)$, $\theta_t = (\pi/2 - \theta)$, τ_{max} is the maximum isometric torque, u_b, u_t are the normalized contraction parameters ($0 \leq u \leq 1$, $u = u_b, u_t$), and α is a constant assumed to be equal for the two actuators. It is easily obtained that $m = I$ for the generalized mass, $b(\dot{\theta}) = 2\beta|\dot{\theta}|$ for the generalized damping, and

$$k(\theta, u) = \alpha(u_b + u_t) - mgl\cos(\theta)$$

for the generalized stiffness. In the latter expression, the role of a gravity-induced term and a co-activation stiffness term are apparent.

If a different actuator model is adopted, namely (cf. [46])

$$\begin{aligned} \tau_b &= -\alpha(\theta_b - \lambda_b)^2, \\ \tau_t &= -\alpha(\theta_t - \lambda_t)^2 \end{aligned} \qquad (3.12)$$

where λ_b, λ_t are interpreted as the rest lengths of the actuators, one has

$$k(\theta) = 2\alpha(\pi - \lambda_b - \lambda_t) - mgl\cos(\theta)$$

45

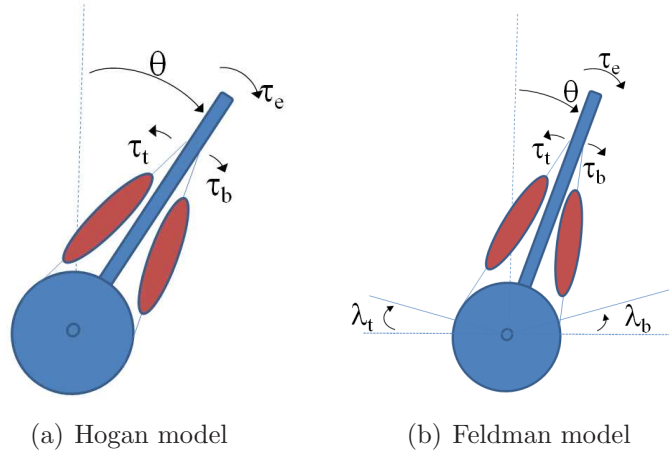(a) Hogan model   (b) Feldman model

Figure 3.3: A link subject to an external load and actuated by two antagonistic actuators. Nomenclature refers to actuator models used in (3.11) and (3.12), respectively.

The values of stiffness and damping for the two examples above, corresponding to time-varying values of the control parameters, are reported in figs. 3.4 and 3.5, respectively.

One of the simplest and most common examples of variable stiffness, both in natural systems and in robotics, is the agonist-antagonist arrangement on nonlinear actuators. To illustrate how our proposed stiffness observer applies to antagonist VSA systems, consider the examples reported above in fig. 3.3. Application of the stiffness observer in this case can be carried out in two ways: 1) the tendon tensions τ_b, τ_t are measured directly, or 2) the external torque $\tau_e(t)$ is measured, and estimates of the link inertia and damping are used. In all cases, a measurement of the link angle $\theta(t)$ is necessary. It should be noticed that, while the first method does not require

3.3 Simulation Results

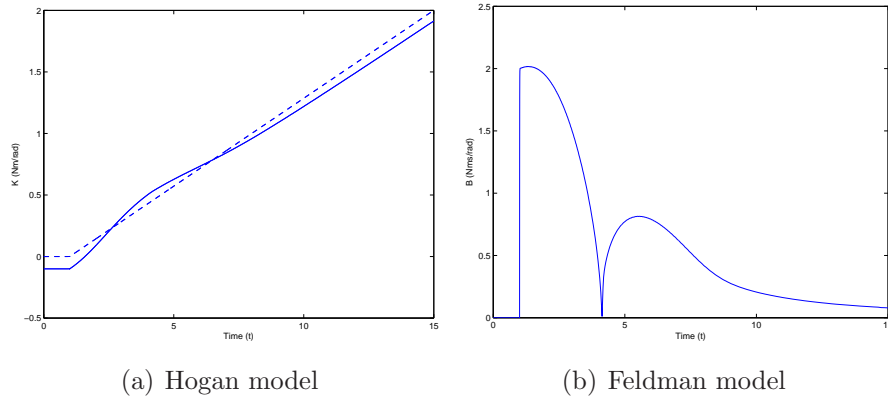(a) Hogan model   (b) Feldman model

Figure 3.4:   Generalized stiffness (left - dashed is without gravity term) and generalized damping for the example with actuators as in (3.11), subject to a unit step in external torque at $T = 1$s, and with time-varying activation $u_b(t) = u_t(t)$ linearly increasing from 0 at $T = 1$s to 1 at $T = 15$s. Numerical values used in simulation: $I = 0.05$Nms^2, $mgl = 0.1$Nm, $\beta = 1$Ns^{2}m, $alpha = 1$Nm/rad, $tau_{max} = 2$Nm.

any estimate of link parameters, it is more invasive in the system, and is inapplicable to e.g. stiffness measurement in a human elbow joint. On the opposite, the second method is easily applicable to this case, although its accuracy will be reduced if poor estimates of inertia and damping are available.

Simulation results for the antagonist arrangements of two muscle-like actuators as described in (3.11) and (3.12) are reported in fig. 3.6 a) and b), respectively. In both simulations, the external force τ_e is a sinusoid with $\omega = 5$ rad/s and amplitude 0.02 Nm. Stiffness is varied during the simulation in a saturated ramp fashion. The ensuing joint

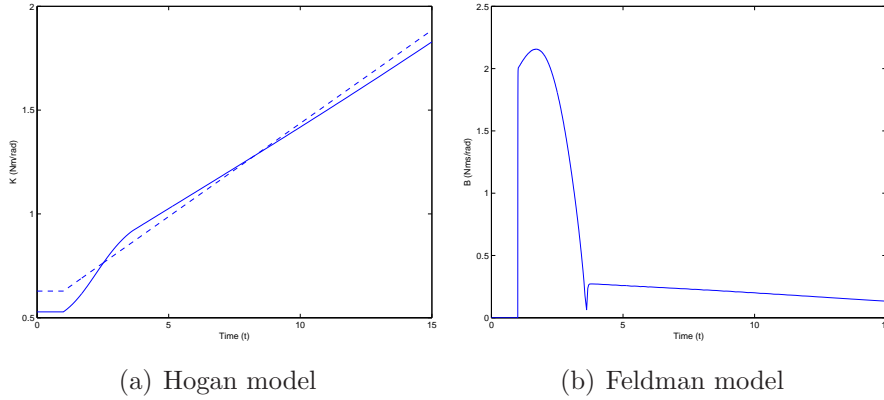(a) Hogan model   (b) Feldman model

Figure 3.5: Generalized stiffness (left - dashed is without gravity term) and generalized damping for the example with actuators as in (3.12), subject to a unit step in external torque at $T = 1$s, and with time-varying reference angle $\lambda_b(t) = \lambda_t(t)$ linearly decreasing from $\pi/3$ at $T = 1$s to 0 at $T = 15$s. Numerical values used in simulation as in fig. 3.4, except for $\alpha = 0.3$.

motion $\theta(t)$ is in the range ± 0.01rad, while $\dot{\theta}$ varies from zero to 0.05 rad/s.

To assess how strongly the performance of the stiffness observer is affected by inertia and damping parameter mismatches (in the case that only external torques are measured), simulations were performed under the hypothesis that m and b were in error by 10% of their actual value. Results reported in fig. 3.7 indicate that, for both muscle models, the relative error on stiffness is of comparable magnitude.
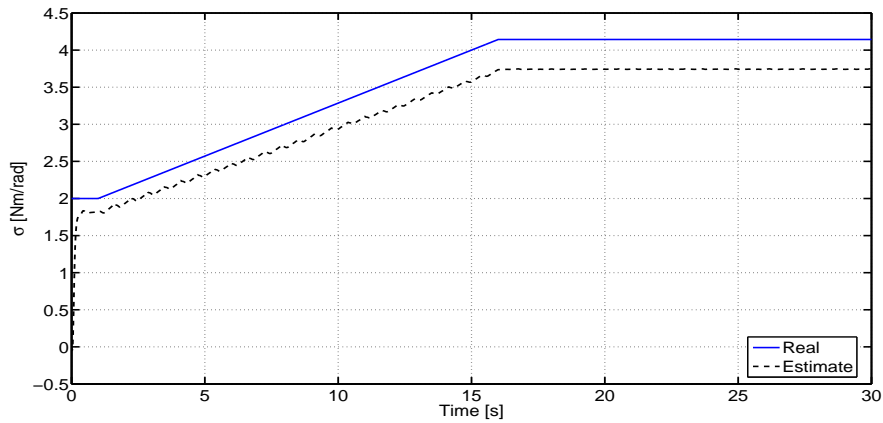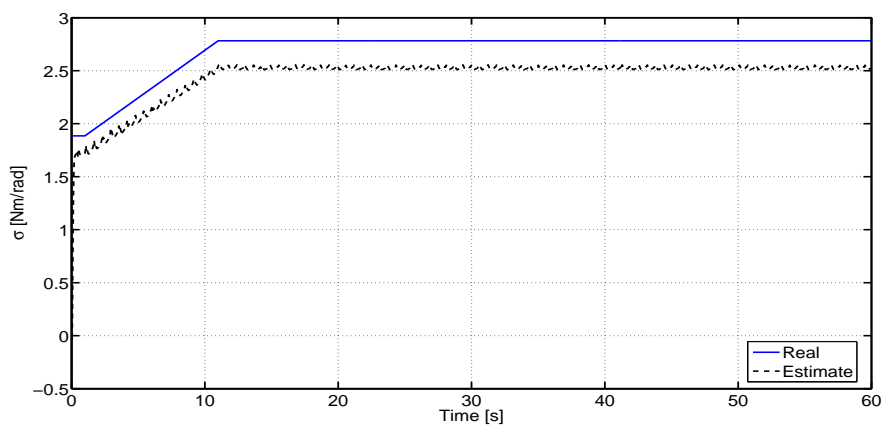
3.3 Simulation Results
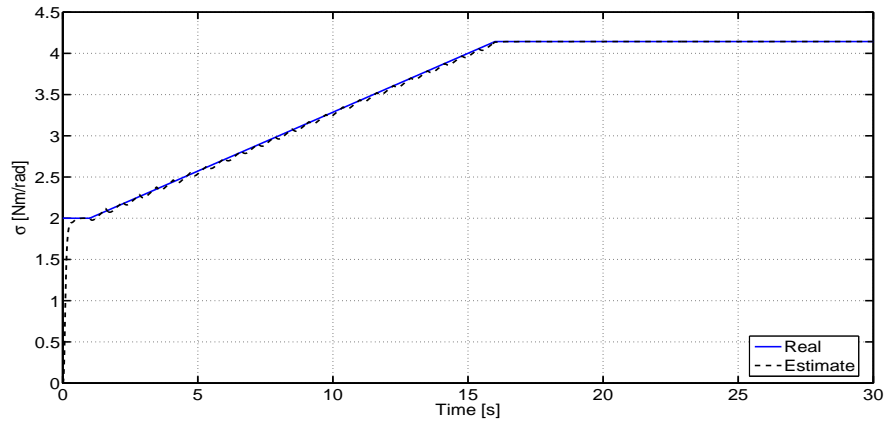
(a) example 1
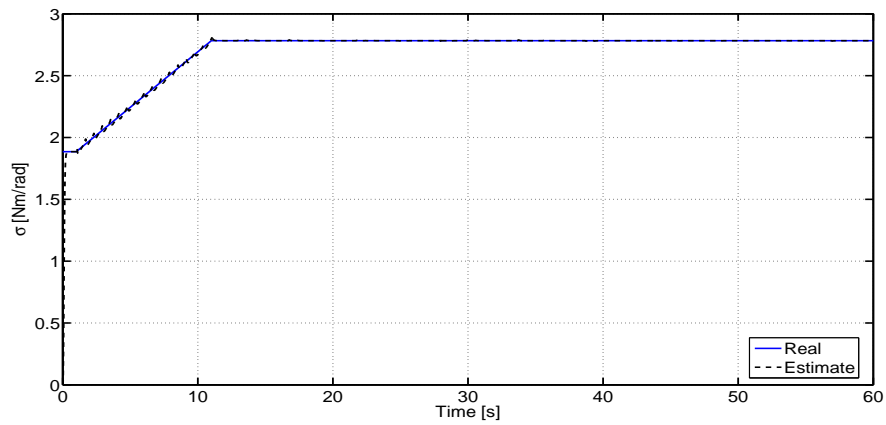
(b) example 2

Figure 3.6: Stiffness tracking for an antagonist VSA system realized adopting nonlinear muscle-like actuators as in equations 3.11 and 3.12 (panels (a) and (b) respectively).

(a) example 1

(b) example 2

Figure 3.7: Stiffness tracking of the antagonist VSA systems with muscle-like actuators as in (3.11) (a), and (3.12) (b), with a 10% error in the knowledge of parameters m and b.

3.3.3   Exponential antagonistic VSA system

Finally, a simulation is reported for the same link actuated by two exponential springs (3.8). In this case, the stiffness is exponentially increasing in time (by linearly varying the co-contraction of the antagonist springs). A sinusoidal external force is applied during the initial and final phases of the experiment, while it is set to zero in the time interval between 10s and 20s. Correspondingly, motion of the links stops ($\dot{\theta} = 0$), and the stiffness estimate is not updated in the interval. When motion resumes, the estimation recovers quickly to the exact value.

3.4   Experimental Results

The algorithm has been tested on the experimental device shown in figure 3.9, implementing the antagonistic VSA device with exponential springs described previously. Two strain-gauge load cells were used to measure the tendon tensions directly, while positions of the link and of the tendon origin were measured using three HEDS-5540 encoders with a resolution of 2000 CPRs. Data were acquired using a National Instruments PCI6251 ADC board for the strain gauges, and an USB-PCI4e for the encoders. Data were sampled with sampling time $T_s = 0.015s$, and afterward filtered with a second–order filter with time constant of $0.02s$. Signal derivatives used in the algorithm were approximated by the numerical filter described by the transfer function

$$D(s) = \frac{s}{1 + 10^{-4}s} \ .$$

(3.13)
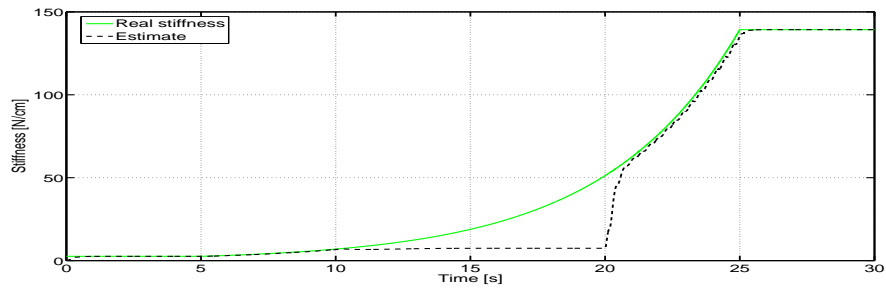
(a) tracking
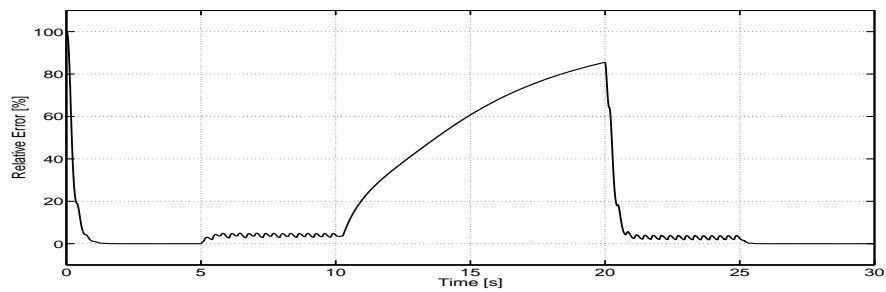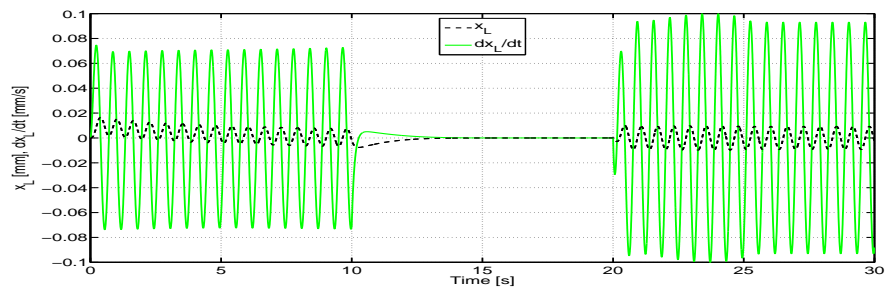
(b) relative error

(c) link movement

Figure 3.8: Simulation Results. Simulation results for the VSA system with exponential springs. a) Comparison of the link stiffness with its estimate; b) Relative estimation error; c) link motion during the simulated experiment.

3.4 Experimental Results

Despite the simplicity of such "Dirty Derivatives" technique, results were suitable for the purposes of the present work, proving the practical feasibility of the proposed method.

It should be pointed out that here the impedance estimates are not used for control in a feedback loop, hence the effect of derivation noise can not destabilize the system.

Input signals derivation could be avoided through use of sensors of the rate of change of desired quantities, e.g. inductive sensors for positions, and piezo-electric sensors for forces.

Both the external load and the torque actuating the tendon tensions were generated manually, and not measured.

To obtain ground-truth data, the mechanical characteristics of the two springs were experimentally evaluated through careful preliminary calibration experiments. The calibration procedure consisted in collecting a large number of force-displacement pairs (x, f), translating them in semi-logarithmic coordinates $(x, y = ln(f))$, finding the regression line in the semi-logarithmic space, such that $y = mx + q$, to finally go back to the original space and obtain $f = e^y = e^{mx+q} = e^q \cdot e^{mx}$, from which $a = m$ and $b = e^q$. From the mean square error of the regression MSE, the relative error margin of the model can be easily evaluate as $r = 1 - e^{MSE}$.

The numeric values of the exponential curves fitting our data are

$$a_1 = 0.999 \quad , \quad b_1 = 3.267 \ ,$$
$$a_2 = 0.950 \quad , \quad b_2 = 2.780 \ ,$$

where subscripts are relative to the two spring. Figure 3.10 shows the regressed curve alongside with experimental data for both the left (a)

and right (b) springs. It is noticeable that, due to un-modeled friction in the mechanism implementing the exponential springs, a certain hysteresis is present, making the model correct only up to a relative error margin of about 25%. Anyway, this error only marginally affected the performance of the proposed observer.

Raw experimental data are reported in fig. 3.11. The estimate of stiffness reconstructed in real-time by the stiffness observer ($\alpha = 3$) is compared with the calibrated stiffness data in fig. 3.12

3.5 Conclusions

In this chapter an algorithm which can be used to observe stiffness in real-time, using force and position sensors was presented. The method's main advantage is the avoidance of any *a piori* knowledge on the model of the physical actuator. This renders it suitable to be applied to any VSA, or other analogous non-linear time-varying stiffness devices, considered as black-boxes.

Simulations and experimental test shown that the method is practically applicable and robust to noisy data and uncertain parameters.

3.5 Conclusions

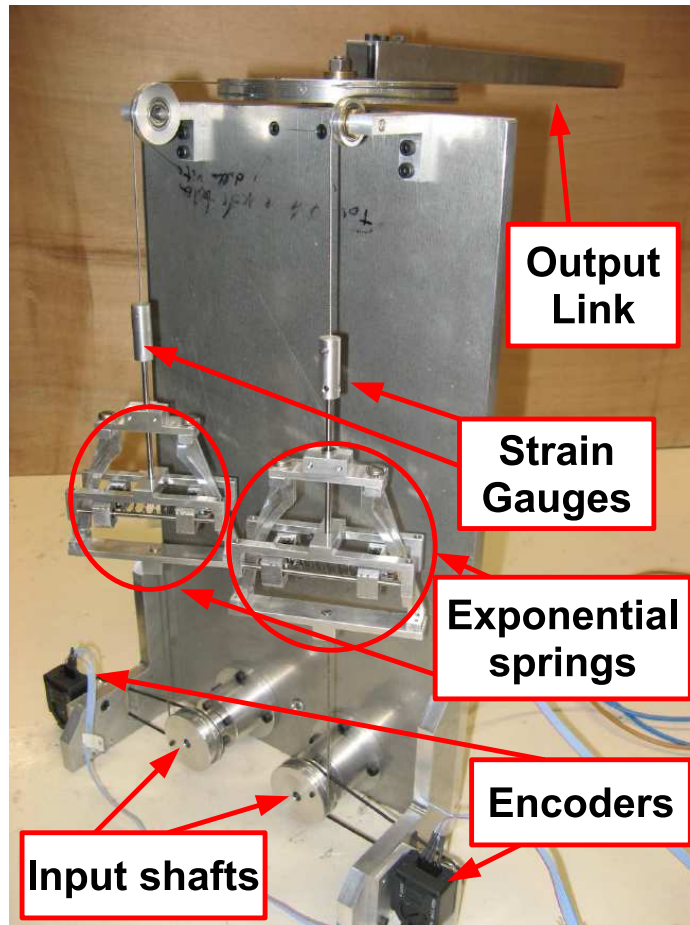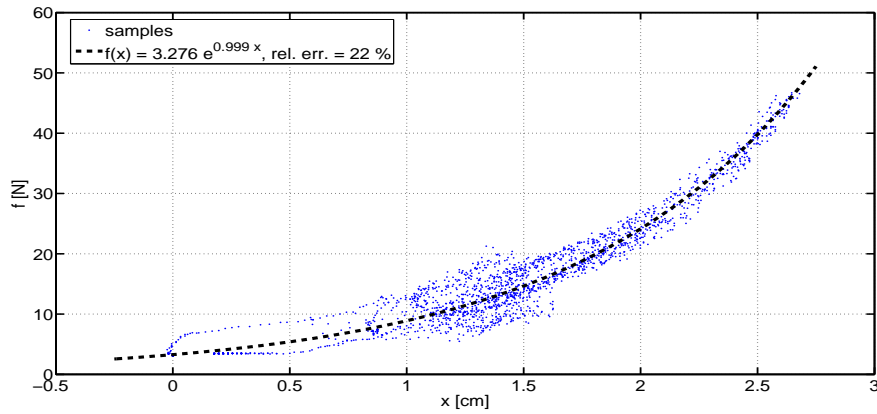Figure 3.9: Experimental setup of the exponential VSA. The setup consists of an antagonistic VSA system with exponential springs, realized using a linear spring forced to move on a suitable cam profile. Force sensors (strain gauges) are mounted on the tendons connecting the springs to the link. Position sensors (encoders) are mounted on the link and on two tendon pulleys coupled with the input levers.

(a) left spring
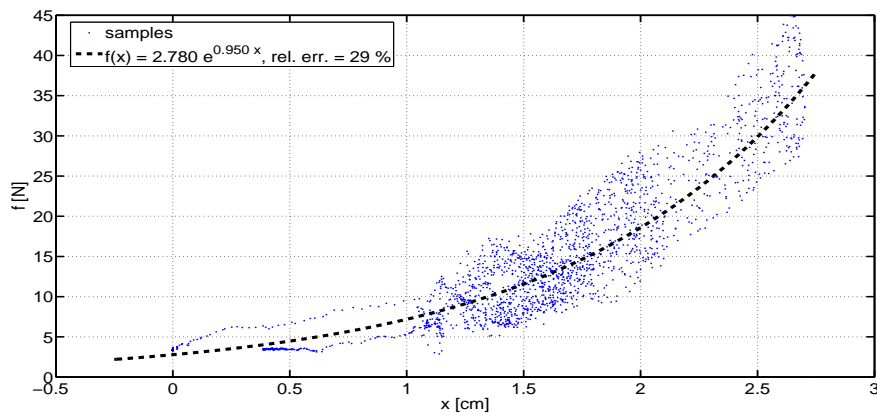
(b) right spring

Figure 3.10: Experimental characterization of the two springs of the exponential VSA. Force and displacement pairs recorded during a calibration experiment, and regression curve are shown for each of the two springs of the experimental VSA system.

3.5 Conclusions
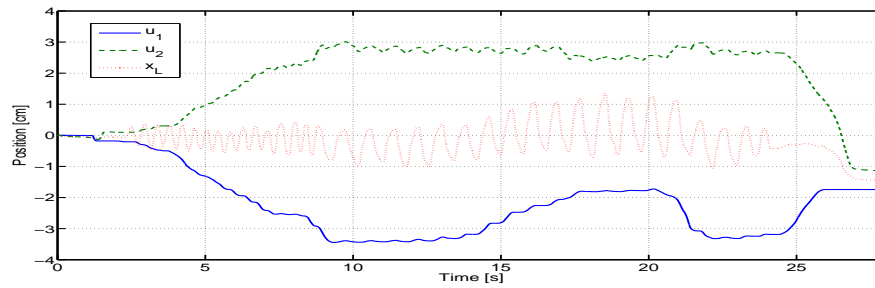
(a) positions
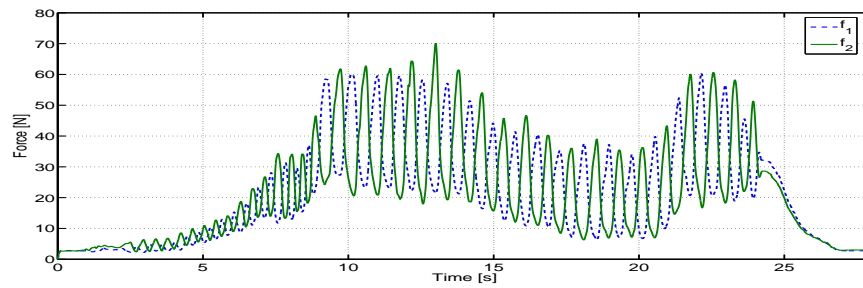
(b) forces
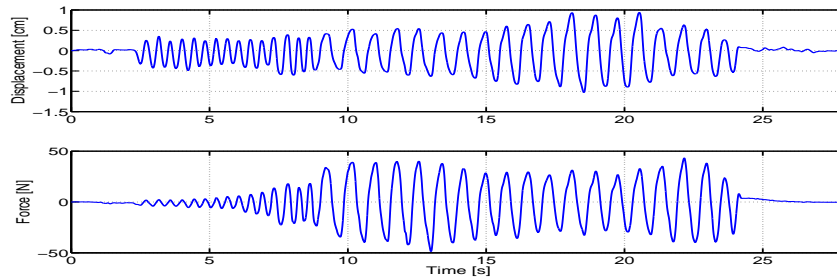
(c) observer inputs

Figure 3.11: Raw data recording from sensors is shown in the first two panels. The third panel shows the values of f and x actually fed to the observer during the experiment.
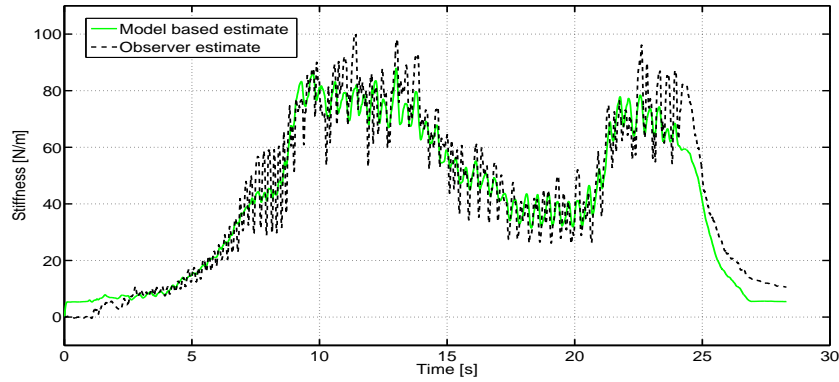
(a) tracking
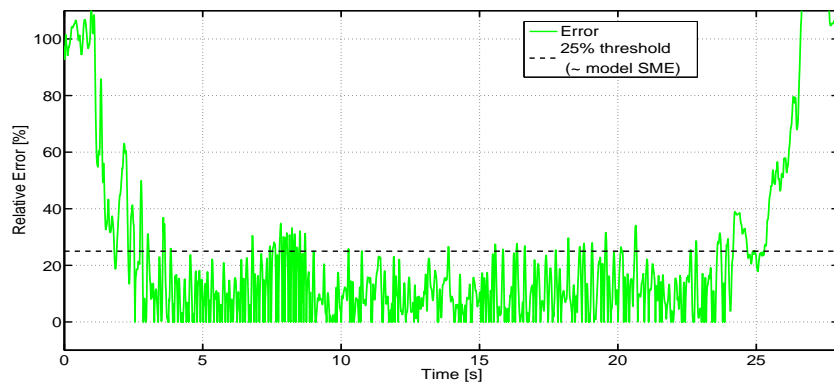
(b) relative error

Figure 3.12: Experimental results for the non-parametric stiffness observer. The first panel shows a comparison between the stiffness values derived by the calibrated spring model and the estimate performed by the stiffness observer algorithm. The second panel shows the relative error (difference between estimator and model, normalized w.r.t. the model) compared with the relative error underlying the model itself.

Chapter 4

Parametric estimation of stiffness

Equations 3.8 and 3.9 defines the limitations of the non-parametric observation approach. A first limitation, somehow intrinsic to the observation problem, is due to fact that the algorithm uses movement of the device to estimate its stiffness, so it cannot estimate when the movement speed is null.

A second limitation to the non parametric approach comes from the dependency of the mechanical characteristic function f on the variable u. In the worst conditions, if the stiffness is changing while outside of observability conditions (i.e. with deflection rate $\dot{u} \to 0$), the change can not be tracked by the non-parametric observer, which simply stops observing (cfr. figure 3.8).

A smarter approach to the observation problem should try to exploit the knowledge of the variable u: Its value is not easily accessible in every situations (as an example consider stiffness identification of

a biological systems), however access to u is, in variable stiffness actuators, given for granted. A VSA, in fact, can be described as mechanical systems with 3 degrees of freedom: one for rest position of the output shaft, one for the configuration of the stiffness adjusting mechanism (u) and one for the deflection of the output shaft from its rest position (y)[1]. Values of those coordinates, or of an equivalent basis, are always measured for feedback control, thus their knowledge should be used to improve estimation performance.

4.1 Derivation of the parametric stiffness observer

A slightly different method can circumvent some of the limitations just mentioned, namely by the adoption of a parametric observer which tries to reconstruct the whole force function $f(y, u)$.

Without loss of generality, group the two inputs of f in a vector form:

$$f(y, u) = f(x), \tag{4.1}$$

assuming now that it is possible to write down the elastic force expression on a series expansion on the vector basis of function space, defined on functions from $\mathcal{R}^2$ to $\mathcal{R}$, one gets[2]

$$f(x) = \sum_{i=1}^{\infty} f_i(x) c_i, \tag{4.2}$$

---

[1] Remember the generic model of a VIA described by 1.23, in section 1.3.

[2] the limitation to $\mathcal{R}^2$ is just practical for our case, but most of the conclusion drawn in this work can be generalized to functions with domain in $\mathcal{R}^n$.

4.1 Derivation of the parametric stiffness observer

where c_i are *constant parameters*.

The above expression can be truncated to the Nth term, obtaining

$$f(x) = \sum_{i=1}^{N} f_i(x)c_i + f_r(x) = c^T f(x) + f_r(x) \qquad (4.3)$$

c and $f(x)$ are column vectors of length N, and $f_r(x)$ is the residual term, neglected with the truncation.

The partial derivatives of $f(x)$ with respect to the elements of the vector x are collected in the row-vector

$$\Sigma = \left[\frac{\partial f(x)}{\partial x_i} \right] = \left[\sigma \,\middle|\, \frac{\partial f(x)}{\partial u} \right]. \qquad (4.4)$$

Exploiting the structure given to the function $f(x)$ by equation 4.3, the above can be rendered as

$$\Sigma = c^T S + \Sigma_r(x), \qquad (4.5)$$

where $S = S(x)$ is a matrix with the derivatives of the elements of the vector f with respect to the elements of x:

$$S = \left[\frac{\partial f_i(x)}{\partial x_j} \right] = \left[\frac{\partial f_i(x)}{\partial y} \,\middle|\, \frac{\partial f_i(x)}{\partial u} \right] = [S_1 | S_2]. \qquad (4.6)$$

The output stiffness to be estimated is one of the partial derivatives contained in Σ, thus if an approximation $\hat{c}$ of the vector c is known, and the residual term $\sigma_r = \frac{\partial f_r}{\partial y}$ is small enough, stiffness can be approximated as

$$\sigma = \Sigma_1 \approx \hat{c}^T S_1 = \hat{\sigma}. \qquad (4.7)$$

To discuss the dynamics of the stiffness estimate, analyze the Lyapunov function and its Lyapunov derivative

$$
\begin{aligned}
V_\Sigma &= \tilde{\Sigma}\tilde{\Sigma}^T & (4.8)\\
\dot{V}_\Sigma &= \tilde{\Sigma}\dot{\tilde{\Sigma}}^T + \dot{\tilde{\Sigma}}\tilde{\Sigma}^T & (4.9)
\end{aligned}
$$

where $\tilde{\Sigma}$ is defined as the estimation error on Σ. Regarding the derivative $\dot{\tilde{\Sigma}}$, it holds

$$
\begin{aligned}
\dot{\tilde{\Sigma}} &\triangleq \dot{\Sigma} - \dot{\hat{\Sigma}} = \\
&= \dot{\Sigma}_r + c^T \dot{S} - \dot{\hat{c}}^T S - \hat{c}^T \dot{S} = \\
&= \dot{\Sigma}_r + \tilde{c}^T \dot{S} - \dot{\hat{c}}^T S. & (4.10)
\end{aligned}
$$

Choose

$$
\dot{\hat{c}} \triangleq S(S^T S)^{-1} A \operatorname{sgn}(\dot{x}) \dot{\tilde{f}} \qquad (4.11)
$$

where here the operation $\operatorname{sgn}(\dot{x})$ is intended component wise, A is a positive definite gain matrix and $\dot{\tilde{f}}$ is defined as

$$
\begin{aligned}
\dot{\tilde{f}} &\triangleq \dot{f} - \dot{\hat{f}} \\
&= c^T S\dot{x} + \Sigma_r \dot{x} - \bar{c}^T S\dot{x} = \\
&= \tilde{c}^T S\dot{x} + \Sigma_r \dot{x}. & (4.12)
\end{aligned}
$$

This implies

$$
\begin{aligned}
\dot{\hat{c}} &= S(S^T S)^{-1} A \operatorname{sgn}(\dot{x})\dot{x}^T \left(S^T \tilde{c} + \Sigma_r^T \right) = \\
&= S(S^T S)^{-1} A \operatorname{sgn}(\dot{x})\dot{x}^T \left(\tilde{\Sigma}^T + \Sigma_r^T \right),
\end{aligned}
$$

4.1 Derivation of the parametric stiffness observer

leading to

$$
\begin{aligned}
\dot{\tilde{\Sigma}} &= \dot{\Sigma}_r + \tilde{c}^T \dot{S} + \\
&\quad - \left[S(S^T S)^{-1} A \operatorname{sgn}(\dot{x}) \dot{x}^T \left(\tilde{\Sigma}^T + \Sigma_r^T \right) \right]^T S \\
&= \dot{\Sigma}_r + \tilde{c}^T \dot{S} - \left(\tilde{\Sigma} + \Sigma_r \right) \dot{x} \operatorname{sgn}(\dot{x})^T A^T (S^T S)^{-1} S^T S \\
&= \dot{\Sigma}_r + \tilde{c}^T \dot{S} - \left(\tilde{\Sigma} + \Sigma_r \right) \dot{x} \operatorname{sgn}(\dot{x})^T A^T.
\end{aligned}
\tag{4.13}
$$

The definiteness of the outer product $P(\dot{x}) = \dot{x} \operatorname{sgn}(\dot{x})^T$, should be discussed. First notice that the matrix, generated by the outer product of two vectors, has all but one of its eigenvalues equal to zero. Being the trace of the matrix equal to the sum of all the eigenvalues, it also equals, in this case, the only non-zero eigenvalue. Looking at the trace of $P(\dot{x})$, it can be easily shown to be

$$
\operatorname{trace}(P(\dot{x})) = \sum_i |\dot{x}_i| \geq 0,
\tag{4.14}
$$

Implying that the matrix $P(\dot{x})$ is non-negative definite.

Going back to

$$
\dot{V}_\Sigma = 2 \left(\dot{\Sigma}_r + \tilde{c}^T \dot{S} - \left(\tilde{\Sigma} + \Sigma_r \right) \dot{x} \operatorname{sgn}(\dot{x})^T A^T \right) \Sigma^T,
$$

it is non-positive definite but for the two terms $\dot{\Sigma}_r \Sigma^T$ and $\tilde{c}^T \dot{S} \Sigma^T$. Suppose that the first can be neglected due to negligibility of the residual term, the convergence of the second to zero and the Persistent Excitation of the trajectory of $x(t)$, that is

$$
\forall t, \delta t :
\tag{4.15}
$$
$$
\alpha_1 I \leq \left(\int_t^{t+\delta t} A \operatorname{sgn}(\dot{x}) \dot{x}^T dt \right) \leq \alpha_2 I
$$

will ensure the convergence of the estimate to the real value of stiffness (see [47] for details).

To check the convergence of $\tilde{c}^T \dot{S}$ to 0, analyze now the dynamic of the error $\tilde{c} = c - \widehat{c}$ with the Lyapunov function, and its Lyapunov derivative:

$$V_c = \tilde{c}^T \tilde{c} \qquad (4.16)$$

$$\dot{V}_c = \tilde{c}^T \dot{\tilde{c}} + \dot{\tilde{c}}^T \tilde{c}. \qquad (4.17)$$

Exploiting the equivalent expression of $\dot{\tilde{f}}$ it holds that

$$\dot{\tilde{c}} = -\dot{\widehat{c}} =$$
$$= -S(S^T S)^{-1} A \operatorname{sgn}(\dot{x}) \dot{x}^T S^T \tilde{c} +$$
$$-S(S^T S)^{-1} A \operatorname{sgn}(\dot{x}) \dot{x}^T \Sigma_r^T \qquad (4.18)$$

the first of the two terms, namely $SMS^T = S(S^T S)^{-1} A \operatorname{sgn}(\dot{x}) x^T S^T$, can be easily shown to be non-negative definite, this because M is the product of

$$(S^T S)^{-1} > 0$$
$$A > 0$$
$$\operatorname{sgn}(\dot{x}) x^T = P^T(\dot{x}) \geq 0$$

and thus is non-negative definite. Once again, when the second term is negligible, the error on the estimate of c is non-divergent, Persistent Excitation of the trajectory, this time in terms of

$$\forall t, \delta t : \qquad (4.19)$$
$$\alpha_1 I \leq \left(\int_t^{t+\delta t} S(S^T S)^{-1} A \operatorname{sgn}(\dot{x}) \dot{x}^T S^T dt \right) \leq \alpha_2 I$$

4.1 Derivation of the parametric stiffness observer

makes the estimate $\widehat{c}$ converge to the correct value.

Going back to the evolution of $\tilde{\Sigma}$, it is important to notice that whenever

$$\|\tilde{c}\|_{\dot{S}\dot{S}^T} < \|c\|_{\dot{S}\dot{S}^T}, \tag{4.20}$$

it yields

$$\|\tilde{c}^T \dot{S}\| < \|c^T \dot{S}\|. \tag{4.21}$$

Note that the right term $\|c^T \dot{S}\|$ of the last equation the variation induced by $\dot{y}$ and $\dot{u}$ on the stiffness, this is the point where the advantage of the parametric observer over the non parametric one becomes clear. Recall, in fact, that in 3.9 the error bound is proportional to $\dot{\sigma}$, one of the two elements of $\dot{\Sigma} = c^T \dot{S}$. Equation 4.21 implies that there exist, in the parametric observer, conditions for which the error bound is smaller than the non-parametric observer error, Those are, in substance, those of equation 4.20.

4.1.1 On the speed of convergence

Equation 4.19 shows, in ultimate analysis, the convergence conditions for the error on the parameters $\tilde{c}$. These alone are enough to imply the convergence of the stiffness estimate, in fact

$$\lim_{\tilde{c} \to 0} \tilde{\Sigma} = \lim_{\tilde{c} \to 0} \tilde{c}^T S = 0. \tag{4.22}$$

However, all the analysis about the error $\tilde{\Sigma}$ was not pointless: remember that analyzing the dynamics of $\tilde{c}$ and $\tilde{\Sigma}$, both cases reduce to negative semi-definite Lyapunov derivative function, and must resort to ask Persistent Excitation conditions to ensure convergence of the error. In both situations the error can decrease just along one

direction of the error space, but an important difference exists: the dimension of the state-space of $\tilde{c}$ is usually much bigger than that of $\tilde{\Sigma}$ which is just of dimension 2. This consideration leads to state that while the convergence speed of the parameters vector $\widehat{c}$ could be slow, convergence of the estimate $\widehat{\Sigma}$ will be, in practice, much faster. Experiments and simulations of latter sections will show it is in fact comparable to the speed of the non-parametric observer.

4.1.2 Overcoming the need for derivatives

One limitation of the current approach is the need for derivatives of signals x and f. Equation 4.22 hints a possibility to overcome it, which consists in building an update law which converges $\tilde{c}$. Such an update law can be built based solely on the prediction error on the estimate of f as follows.

Given an estimate $\widehat{c}$ of the vector c, an estimate of the force f can be built as $\widehat{f} = \widehat{c}^T F$, where $F = F(x)$ as in equation 4.3, from which the error $\tilde{f}$ for which holds

$$\tilde{f} \triangleq f - \widehat{f} = F_r(x) + c^T F - \widehat{c}^T F = F_r(x) + \tilde{c}^T F \ . \tag{4.23}$$

Defining an update law

$$\dot{\widehat{c}}_* \triangleq \alpha (F^T F)^{-1} F \tilde{f}, \tag{4.24}$$

where B is a positive definite gain matrix (the subscript $*$ is used to distinguish from the update law in 4.11), yields for the dynamics of the $\tilde{c}$

$$\begin{aligned}
\dot{\tilde{c}} &= -\dot{\widehat{c}} = -\alpha (F^T F)^{-1} F \left(F_r(x) + \tilde{c}^T F \right) = \\
&= -\alpha (F^T F)^{-1} F F^T \tilde{c} - \alpha (F^T F)^{-1} F F_r(x),
\end{aligned}$$

4.1 Derivation of the parametric stiffness observer

which renders the derivative of the Lyapunov function V_c of equation 4.16 non-positive definite provided that the truncation error term $F_r(x)$ is negligible. Persistent excitation in terms of

$$\forall t, \delta t : \ \alpha_1 I \leq \left(\int_t^{t+\delta t} \alpha (F^T F)^{-1} F F^T dt \right) \leq \alpha_2 I \qquad (4.25)$$

will make the estimate $\widehat{c}$ converge on the real value c. Convergence of vector $\widehat{c}$ yields convergence of the parametric model to the real mechanical characteristic represented by the function $f(x)$; this, by virtue of 4.22, yields convergence of estimation of stiffness calculated as $\widehat{c}^t S_1$. Nevertheless, deriving the innovation from the error $\tilde{f}$ instead of $\dot{\tilde{f}}$, prevents considerations on convergence speed similar to those derived in section 4.1.1. This translates, in practice, in a slower convergence of the estimate of the stiffness value. Given a point x where to measure stiffness, the estimate becomes accurate only after the model has converged in the whole neighborhood x. This renders, at the moment, the derivative-free approach less feasible for real-time measurements like those needed for closed loop control, unless an already accurate initial guess for the vector c is available.

4.1.3   On the choice of the Function basis

The discussions of this section are abstract from the particular function basis chosen to represent the function $f(y, u)$. The only strict requirements lie on the differentiability of the functions composing the basis, such that the matrix S can be derived from the vector f. Nevertheless, a deeper analysis of this aspect of the problem could lead to improvement on the performance of the estimator.

The simplest aspect to consider is that the error dynamic is excited by the value of the residual term $f_r(y, u)$ and its derivative, a good choice for the function basis should take this into account thus, whenever some information on the shape of the function $f(y, u)$ exists, the designer of the estimator should pick a basis where the function f can be represented exactly by a finite set of basis elements $f_i(y, u)$, or otherwise, minimizing the approximation error.

For the sake of this recall that, given both a domain for the values of (y, u), and a scalar product between functions defined on this domain, there exists a basis whose elements are orthogonal with respect to the aforementioned scalar product and have unit length in the norm induced by it, this ensures that

$$< f_i(y, u), f_r(y, u) > = \ 0.$$

4.2 Simulation Results

In this section results of the proposed stiffness observer are presented and compared with the performance of the non-parametric method.
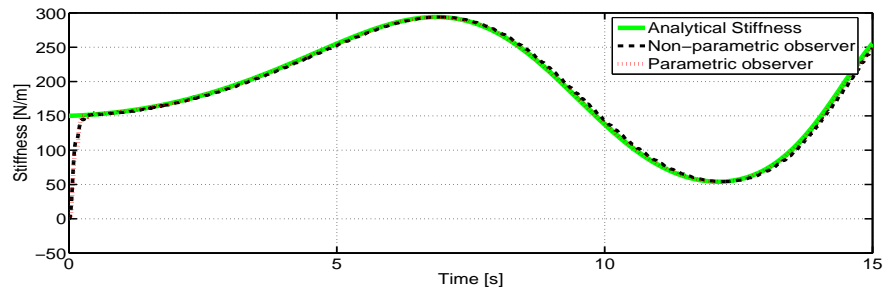
4.2.1 Exact Model Parametric identification

In this first application the parametric observer is applied to estimate the stiffness of an Agonist-Antagonist VSA mechanism realized with two identical cubic springs, whose force-displacement characteristic is described by
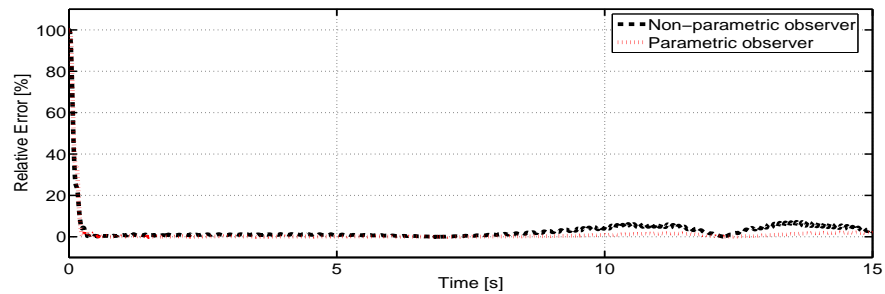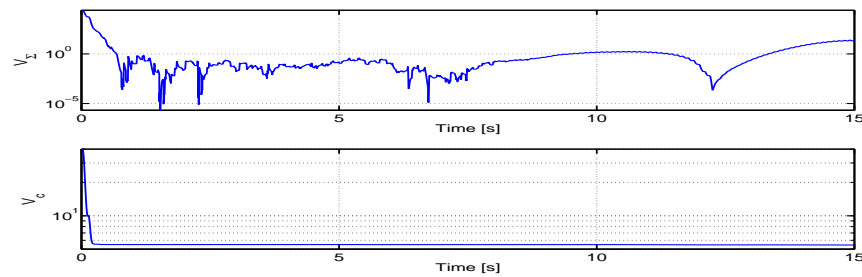
$$f = (y_i - y_L)^3.$$

4.2 Simulation Results

(a) stiffness tracking

(b) relative error

(c) Lyapunov functions

Figure 4.1: Performance of the parametric and non-parametric observers tracking the stiffness of an A-A VSA system featuring a stiffness function which is completely representable on the truncated basis of adopted by the parametric observer.
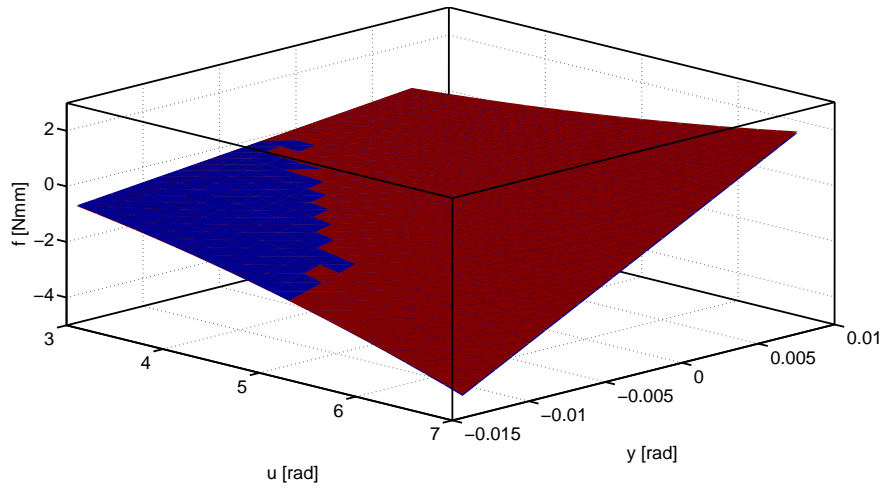
(a) Approximation of the force function
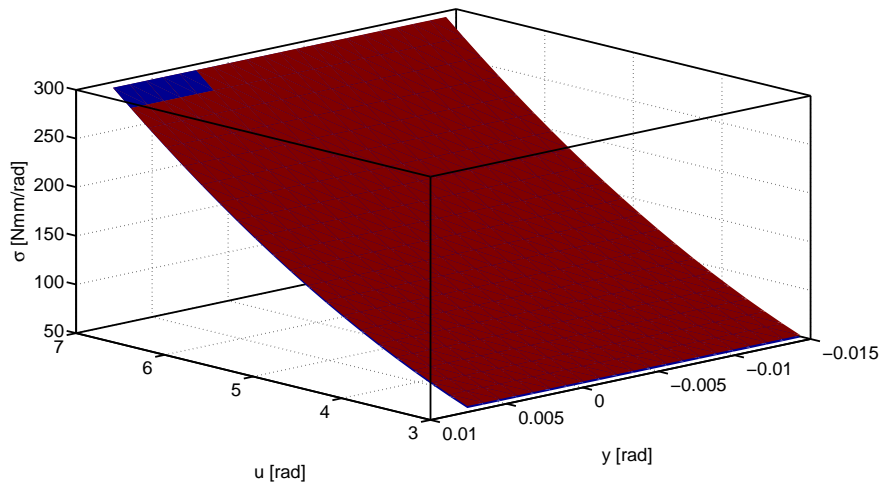
(b) Approximation of the stiffness function

Figure 4.2:   Reconstruction of the functions describing the recoil force and the stiffness of the system. Blue color is used for the real functions and red color for the estimate ones respectively.

4.2 Simulation Results

This determines a VSA system where the equilibrium point of the link is, in the absence of external loads, in the middle position $y_E = (y_1 + y_2)/2$. The link deflection y, in consequence, is quantified by $y = y_L - y_E$. The configuration of the stiffness can be easily described by completing the configuration space of the mechanism, for example with the variable $u = (y_2 - y_1)/2$. Under these hypotheses the force-displacement characteristic of the system can be easily shown to be

$$f(y, u) = (2y^3 + 6yu^2).$$

As a consequence, the stiffness function is

$$\sigma(y, u) = 6(y^2 + u^2).$$

This particular function can be completely represented on a function basis of the kind

$$f_k(y, u) = y^i u^j \text{ with } k = \left((i - j)^2 + i + j\right)/2, \qquad (4.26)$$

using only the first 9 elements of the basis, by

$$c = [0\,0\,0\,0\,0\,0\,2\,6\,0\,\cdots]^T.$$

This ensures that if expressing the function with at least 9 terms of the basis 4.26 the residual term f_r and its derivatives are null.

The parameters of the two observers are set as follows: for the non-parametric observer, the gain is set to $\alpha = 100$, for the parametric one, the first 10 elements of the basis in equation 4.26 are adopted, and the gain matrix is set to $A = 100I$.

Results are shown in Fig. 4.1: both techniques exhibit analogous satisfactory performance as expected. Panel (c) of Fig. 4.1 shows

the time evolution of the Lyapunov functions V_Σ and V_c on a semi-logarithmic scale: as expected the magnitude of V_c is always non-increasing but after a fast start its convergence speed is sensibly slowed down. The magnitude of V_Σ, on the other hand, is not always decreasing because of the influence of $\tilde{c}\dot{S}$, but, in practice, it is much faster, shrinking its magnitude by two orders in the first few seconds, and remaining contained afterwards.

The two panels on Fig. 4.2 show a comparison of the reconstructed model in term of the functions $\widehat{f}$ and $\widehat{\sigma}$ with the real one, highlighting a good conformance between the two.

4.2.2   Inexact Model Parametric identification

In this second simulated experiment, both observers are used to track the stiffness of an Agonist-Antagonist VSA, realized with exponential springs, as described in section 3.3.3. It is characterized by the force and stiffness functions

$$
\begin{aligned}
f(y,u) &= k(e^{y+u} - e^{u-y}) & (4.27) \\
\sigma(y,u) &= k(e^{y+u} + e^{u-y}). & (4.28)
\end{aligned}
$$

The gain of both observers is kept the same as in the previous simulation, but the state-space of the parametric observer is increased, using up to the 15th element of the function basis of equation 4.26. This modification is introduced to face the fact that the exponential functions of equation 4.28 can not be completely represented over a finite sub-set of this basis, and thus, to render the residual term small enough.

4.3 Experimental Results

Results are shown in Fig. 4.3. Notwithstanding the imperfect representability of the function over the chosen function basis subset, the parametric observer performance keeps satisfactory.

Another important result is visible in the second simulation, which is an advantage of the parametric observer over the non-parametric one. Looking at the two time intervals $[10, 20]s$ and $[40, 50]s$ in Fig. 4.3(c), it can be noted that the evolution of y stops: this leads to a drop of the convergence conditions of the non-parametric observer, which simply stops observing. The parametric observer, on the other hand, is building its estimate also on the knowledge of u. Thanks to the model it learned already, it keeps estimating the stiffness of the system even in those adverse conditions. The error is sensibly lower justifies the increased complexity of the algorithm.

4.3 Experimental Results

Results, reported in Fig. 4.4, show the substantial similarity between the performance of the two methods. Nevertheless, the advantage of the parametric approach, exposed in previous sections, is evident once again: due to the drop of speed of y in conjunction with a tangible change in u after time $t = 24s$, the non-parametric observer suffers for a drop of performance. The parametric observer on the other hand, exploiting the information relative to u, and the collected information about the model, does not suffer from this inconvenience, keeping the relative error small, comparable to the model reliability threshold of 25%.
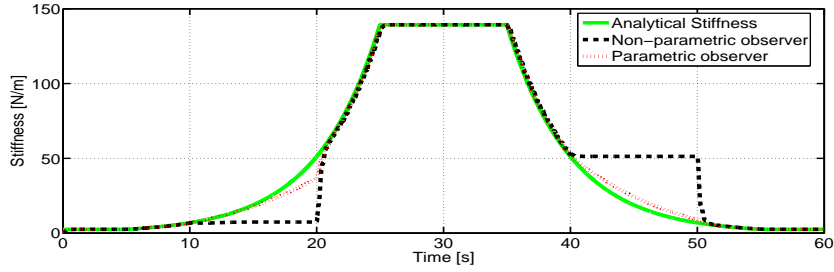
(a) stiffness tracking
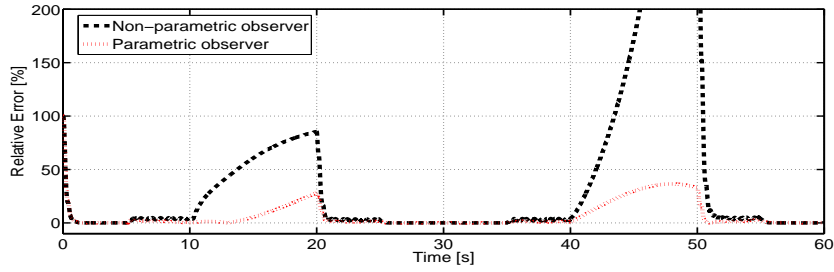
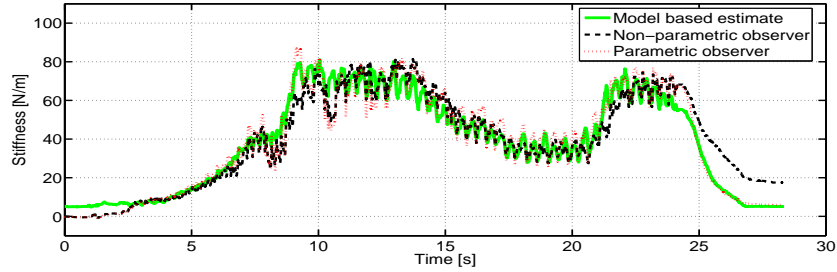(b) relative error
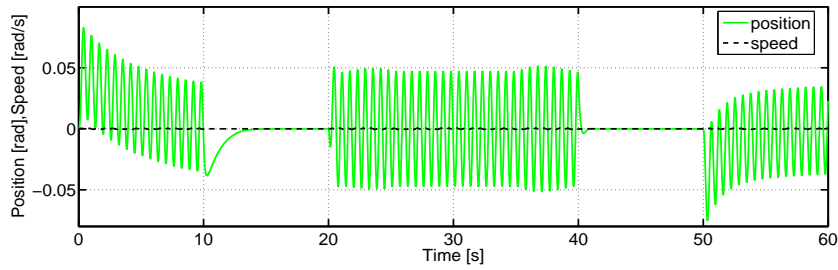
(c) link movement

Figure 4.3: Parametric and non-parametric observers tracking the stiffness of an AA VSA system whose stiffness function has $f_r \neq 0$. The information learned in the first few seconds, allows the parametric observer a low error even between $[10, 20]s$ and $[40, 50]s$ when the system trajectory does not allow a good bound for the non-parametric estimate.

4.3 Experimental Results

(a) stiffness tracking
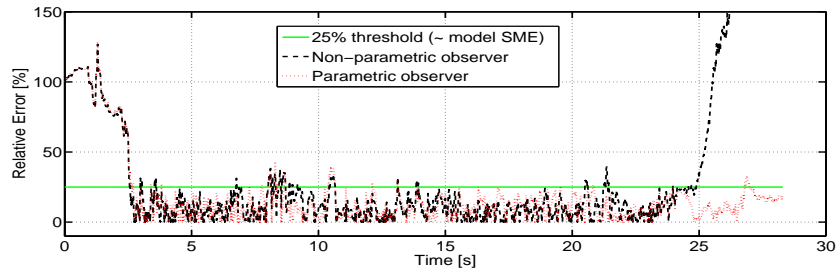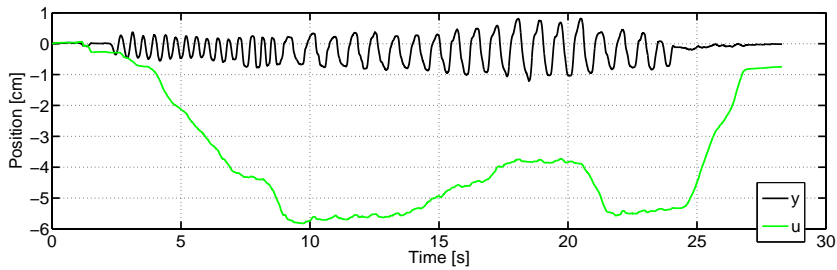
(b) relative error

(c) evolution of y and u

Figure 4.4: Experimental results obtained using the parametric and non-parametric algorithm are compared in terms of tracking and relative error on panels a and b, in panel c the evolution of y and u is shown. The performance of the two observers is similar for most of the experiment but differ in favor of the parametric observer after second 24.

4.4 Conclusions

This chapter presented a parametric observer designed to measure the non-linear, time-varying stiffness of a VSA device, using force and position sensors. The method is an evolution of the non-parametric observer presented in previous chapter. At the cost of using a wider state-space the proposed solution is proven to present two main advantages over the former one: the possibility to use the measurement of the stiffness-setting angle, and the capacity to reconstruct the shape of the stiffness function.

A final interesting aspect of this algorithm is the possibility not to use the derivative of the input signals, however this would slow down the speed of convergence.

Conditions for the convergence of the algorithm were derived and then performance of the observer was compared with results obtained with the former approach, both with simulations and experimental data.

Chapter 5

Estimation of Impedance

In this section the approach of section 3 is extended, integrating it with an extended Kalman filter, to estimate, along with the non-linear and fast time-varying stiffness component of the impedance, the linear components due to inertia and damping. Two techniques are proposed to realize this idea, and the advantages of the two approaches are briefly described.

The results of this approach have been tested on the AwAS Variable Stiffness Actuator, a prototype of VSA developed within the Italian Institute of Technology, a picture of which is shown in figure 5.2.

5.1   Combined EKF-Stiffness Observer

By differentiating the link dynamics in equation 1.23 with respect to time, yields

$$\dot{\tau}_{ext} = I\,\dddot{q} + N\ddot{q} + \sigma(\dot{q} - \dot{\theta}_1) + F_u\dot{\theta}_2, \tag{5.1}$$

Assuming that a measurement of the torque τ_{ext} is known, a possible approach to the combined estimation problem relies on the juxtaposition of a stiffness observer and an EKF. Rewriting equation 5.1 as

$$\dot{\tau}_{ext} - \sigma(\dot{q} - \dot{\theta}_1) - F_u\dot{\theta}_2 = \dot{\tau}_* = I\dddot{q} + N\ddot{q} , \qquad (5.2)$$

an EKF can be easily built in to estimate the impedance parameters of the rightmost side given a measurement of $\dot{\tau}_*$. Given the estimates $\hat{I}$ and $\hat{N}$ derived from the EKF, the estimation of stiffness can be obtained by using the best-effort prediction for the $\dot{\tau}_{ext}$ defined now as

$$\dot{\hat{\tau}}_{ext} = \hat{I}\dddot{q} + \hat{N}\ddot{q} + \hat{\sigma}(\dot{q} - \dot{\theta}_1) , \qquad (5.3)$$

where $\hat{\tau}_{ext}$, $\hat{I}$, $\hat{N}$ and $\hat{\sigma}$ are the estimations of external torque, inertia, damping and stiffness, respectively.

By virtue of the robustness of the non-parametric stiffness observer, the error on the knowledge of I and N should introduce only an error on the estimate σ.

The knowledge of $\dot{\tau}_*$ is, unfortunately, unavailable but, possessing possessing an estimate of the stiffness σ, can be approximate as

$$\dot{\hat{\tau}}_* = \dot{\tau}_{ext} - \hat{\sigma}(\dot{q} - \dot{\theta}_1).$$

This approach has the advantage of estimating the whole set of parameters using only torque and position measurement (and their derivatives) without needing any other assumption. It works under the hypothesis that the initial error on the estimates of I and N and the influence of the term F_u are small enough. Nevertheless, the problem of an interaction loop between the two observers arises. This has a negative effect on the stability of the algorithm, and can

make convergence depend strongly on initial guesses. A solution to this problem is presented in the next section (5.2).

5.2   Decoupled Impedance observer

Assume that the torque sensor necessary for the stiffness estimation is assembled between the actuator unit and the link so as to measure Σ. It is possible to notice, that the variable impedance term Σ, giving rise to the stiffness σ, appears in both the first and second equations of (1.23). Considering, in particular, the second equation of (1.23), its general form is identical to that needed by the stiffness observer. While accomplishing the stiffness estimation task on the first equation of (1.23) requires the knowledge of I and N, performing the estimate on the second of (1.23) demands just the knowledge of the motor parameters B_1 and D_1. Those values can be usually deduced by the motor data-sheets, or otherwise measured with standard off-line calibration techniques [1]. The rest of the problem, i.e. the estimation of the inertia I and the damping N, can be realized with a standard EKF on the system

$$I\ddot{q} + N\dot{q} = \hat{u}. \tag{5.4}$$

---

[1]Moreover, small errors in the knowledge of these two parameters are robustly tolerated.

Defining the extended state vector

$$
\begin{bmatrix} q \\ \dot{q} \\ 1/I \\ N/I \end{bmatrix} = \begin{bmatrix} x_1 \\ x_2 \\ x_3 \\ x_4 \end{bmatrix}, \tag{5.5}
$$

allows to write the non linear discrete state representation of (5.4) as

$$
\begin{cases} x_1^{(k+1)} = x_2^{(k)} T_c + x_1^{(k)} \\ x_2^{(k+1)} = (-x_3^{(k)} x_2^{(k)} - x_4^{(k)} \hat{u}^{(k)}) T_c + x_2^{(k)} \\ x_3^{(k+1)} = x_3^{(k)} \\ x_4^{(k+1)} = x_4^{(k)} \end{cases}, \tag{5.6}
$$

where T_c is the sampling time. From (5.6), a suitable EKF can be designed which is effectively decoupled from the stiffness observer (for some details see the appendix or [48]). The stiffness observer, built in as explained in section 3, is discretized such as

$$
\hat{\sigma}^{(k+1)} = [\alpha \dot{\hat{\Sigma}} \mathrm{sgn}(q^D - \theta_1^D)] T_c + \hat{\sigma}^{(k)}, \tag{5.7}
$$

with $\dot{\hat{\Sigma}}$ defined as

$$
\dot{\hat{\Sigma}} \triangleq \Sigma^D - \hat{\sigma}^D (q^D - \theta_1^D) - B_1 q^{DD} - D_1 q^{DDD}, \tag{5.8}
$$

with x^D calculated, for a generic quantity x, as

$$
[x^D]^{(k)} = \frac{x^{(k)} - x^{(k-1)}}{T_c}. \tag{5.9}
$$

5.3   Results

The impedance observer was tested through simulations and experiments on the Actuator with Adjustable Stiffness (AwAS), developed by the Italian Institute of Technology [11] (see Fig. 5.2). The dynamics of the AwAS actuator, neglecting the gravity, can be described by the following equations:

$$
\begin{cases}
I\ddot{q} + N\dot{q} + \tau_E = \tau_{ext} \\
B_1\ddot{\theta}_1 + D_1\dot{\theta}_1 - \tau_E = \tau_1 \\
B_2\ddot{\theta}_2 + D_2\dot{\theta}_2 + \tau_r = \tau_2
\end{cases}
\tag{5.10}
$$

where I, N and M are the inertia, damping and mass of the link with generalized coordinate q; B_i, D_i and τ_i with $i \in [1, 2]$ are the inertia damping and command torque of the motors M_1 and M_2, respectively, with generalized coordinate θ_i. The external torque applied at the joint is represented with τ_{ext} and the elastic torque τ_E is formulated such as

$$
\tau_E = k_s r^2 \sin(2\theta_s)
\tag{5.11}
$$

where k_s is the spring rate and $\theta_s = q - \theta_1$ is the spring deflection; the rotational stiffness $\sigma = \frac{\partial \tau_E}{\partial \theta_s}$ is therefore obtained such as

$$
\sigma = 2k_s r^2 cos(2\theta_s).
\tag{5.12}
$$

The joint stiffness σ depends on the lever arm r, which is the effective distance between the center of rotation of the joint and the springs, and, in minor contribution, from the deflection of the springs. The lever arm is adjusted through a ball screw mechanism through the actuator M_2 such as

$$
r = r_0 - n\theta_2
\tag{5.13}
$$

where n is the transmission ratio between the motor and the ballscrew and r_0 is the initial length. Finally, the torque τ_r which applies at the motor M_2 is given by

$$\tau_r = -2k_s n r sin(\theta_s)^2. \qquad (5.14)$$

Note that, to simplify the notation the motors inertia and damping factors are already scaled by the transmission ratios.

5.4 Tuning

The observer was calibrated by trial and error as following.

1. Extended Kalman Filter: starting from matrices Q, R e $P_{0|0}$ (they are process noise covariance and observation noise covariance and initial guess covariance respectively) equal to the identity, diagonal elements related to badly converging variables are tuned. [2]

2. Stiffness observer: the only parameter to calibrate is the observer gain α, it is obtained by optimizing the trade-off between the effects of the measurement noise on one side, and speed of convergence of the estimate on the other.

---

[2]In particular, elements of Q are related to oscillation of the variables, elements of R (refer to textbooks as [48] for details) to the convergence speed. $P_{0|0}$, influences the update speed on the initial moments in which EKF starts.
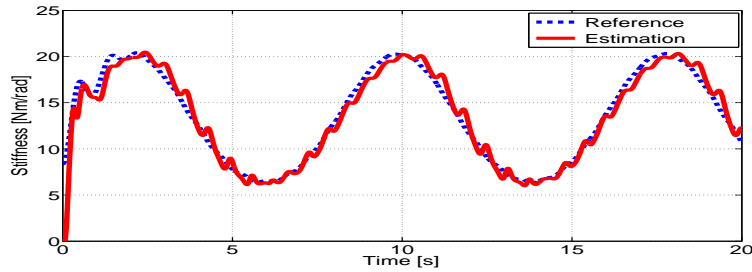
5.5 Simulations

Results of simulations are shown in Fig. 5.1. The simulated experiment consisted in feeding the two motors of the AwAS actuator with two sinusoidal torque signals.

5.6 Experimental Setup

The setup of the AwAS system, employed for the execution of the experimental trials, is shown in Fig. 5.2. The AwAS unit consists of two actuators. The main joint actuator (Link Motor) is based on a combination of an Emoteq HT-2300 frameless brushless motor (capable of a peak torque of 2.3Nm) and a harmonic reduction drive CSD 20 (reduction ratio of $N = 50$ and peak rated torque of 80Nm). The stiffness adjusting actuator (Stiffness Motor) is realized by a DC motor from Faulhaber (peak torque of 0.8Nm) combined with a ball screw reduction drive which converts the rotary motion of this motor into a linear displacement, allowing to change the effective lever arm and efficiently tune the joint stiffness. More details on the mechanical implementation of the AwAS unit can be found in [49]. The sensing system of AwAS includes four position sensors and one torque sensor; one optical encoder measures the position of the link motor, two absolute magnetic encoders measure position of the joint before (at the harmonic drive output) and after the compliance module (link position) while an incremental encoder monitors the position of stiffness motor and subsequently the displacement of the linear drive. A torque sensor is located between the harmonic drive and the intermediate link and senses the torque applied by the link
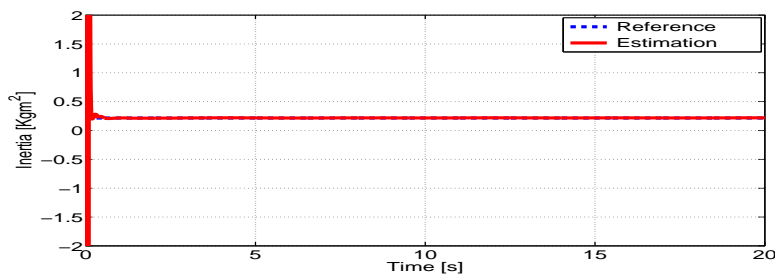
(a) Stiffness estimation
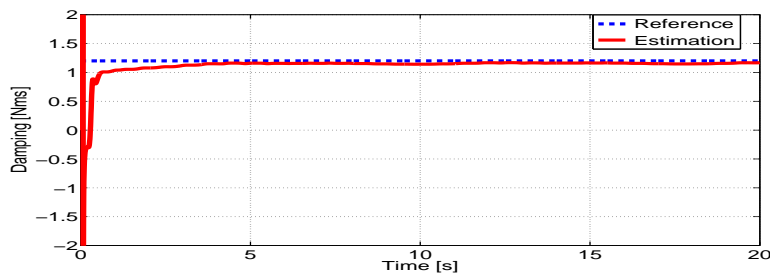
(b) Damping estimation

(c) Inertia estimation

Figure 5.1: Impedance observer simulation results. Mean values of relative errors: 5.1% for the link stiffness, 6.7% for link damping and 9.8% for link inertia.

motor. The general specifications of AwAS are presented in Table 5.1. The unit controller and power driver used to control the AwAS unit are custom control boards based on the Motorola DSP 56F8000 chip with CAN communication interface.

Table 5.1: General specification of AwAS

Range of Motion(deg)	-120÷120
Range of Stiffness (N m/rad)	30÷130
Peak Output Torque (N)	80
Length (m)	0.27
Width (m)	0.13
Total Weight (Kg)	1.8

5.7   Results Discussion.

Results of simulations are shown in Fig. 5.1, while results of experiments are presented in Fig. 5.3. The main differences that can be noticed consist in a slower convergence speed and a larger error on the stiffness estimate. They arise mostly due to the quantization error on the position sensor, which has a negative relapse on the calculation of the derivatives, and force the gains to be smaller.

5.8   Conclusions

This chapter proposed the development of an impedance observer for Variable Impedance Actuators, designed by combining a stiffness observer for non-linear systems, and an Extended Kalman Filter. It was shown how the clever placement of the torque sensor on the VIA device allows decoupling the two observers, thus avoiding possible instability issues that could arise from the interaction of the two observation dynamics.

The resulting observer was successfully tested on the AwAS variable stiffness actuator, in numerical simulation in a first phase, and in physical experiments subsequently.

5.8 Conclusions
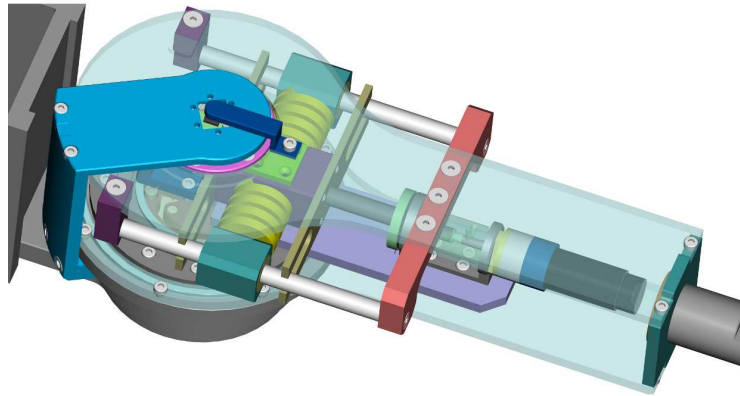
(a) AwAS CAD
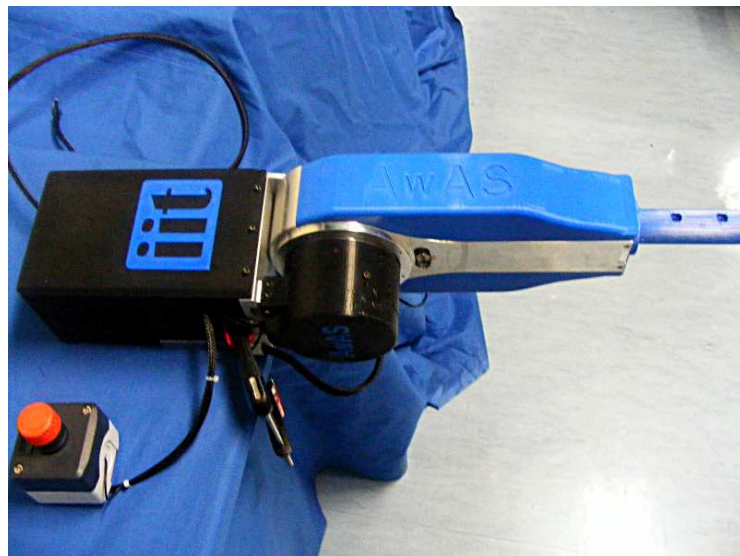
(b) AwAS real prototype

Figure 5.2: The AwAS, Actuator with Adjustable Stiffness.

(a) Stiffness estimation

(b) Damping estimation

(c) Inertia estimation

Figure 5.3: Impedance observer experimental results. Mean values of relative errors: 38.2% for the link stiffness, 9.4% for link damping and 12.2% for link inertia.

Conclusions
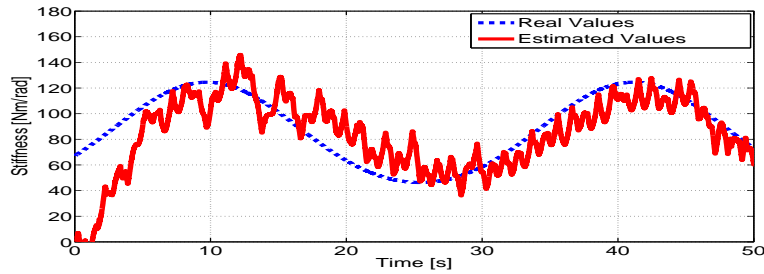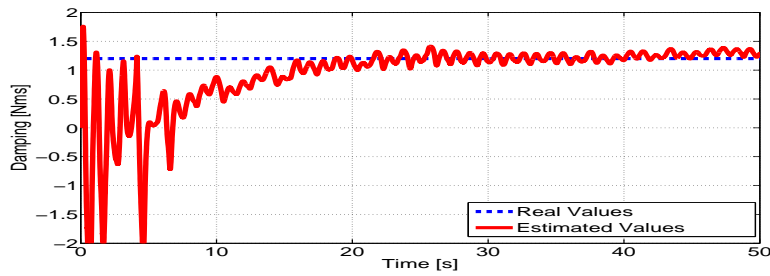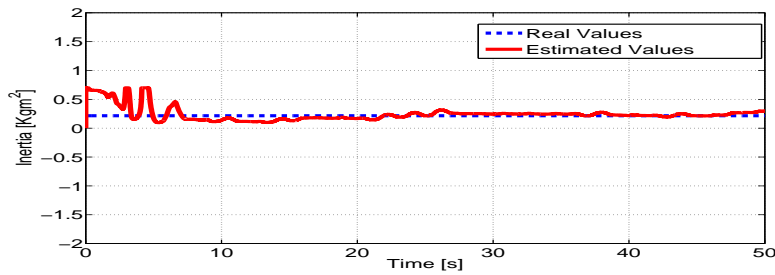
This thesis analyzed the problem of controlling a VIA and pointed out the lack of a reliable way to implement closed-loop control of the passive impedance of the VIA. This problem is due to the absence of sensor which can measure mechanical impedance on-line.

Therefore, an innovative approach was proposed to observe on-line the impedance of a VIA based on available force and position measurements.

In particular, three embodiment of the observer idea were presented. The first is a non-parametric stiffness observer, for which convergence bounds were derived, and which was shown to estimate on-line the stiffness of a VSA with an error comparable to the reliability margins of the stiffness derived from off-line model identification of the same device.

Second, a parametric stiffness observer was shown, which is an evolution of the previous approach. The parametric observer, at the cost of a slightly more complex structure, is able to improve the performance of the non-parametric approach in different aspects. Especially, it is able to learn, over time, the shape of the whole mechanical characteristic function. This in turn allows for the non-

parametric observer to extrapolate the estimate even during time intervals when lack of excitation does not guarantee good estimate bounds to the non-parametric observer. Simulation and experiments were reported to illustrate either this and other peculiarities.

Finally, it was shown, in a third and final version, how the stiffness observer can be integrated with other existing approaches, in particular EKF, to estimate either non-linear time-varying stiffness, and linear damping and inertia coefficients of the link-side dynamic of a VIA-powered robot. Experimental results were shown to validate the approach.

Bibliography

Author's bibliography

[A1] R. Schiavi, G. Grioli, S. Sen, and A. Bicchi. VSA-TWO: A novel prototype of variable stiffness actuator for safe and performing robots interacting with humans. In *Proc. IEEE Int. Conf. on Robotics and Automation*, pages 2171 – 2176, 2008.

[A2] A. Bicchi, M. Bavaro, G. Boccadamo, D. De Carli, R. Filippini, G. Grioli, M. Piccigallo, A. Rosi, R. Schiavi, S. Sen, and G. Tonietti. Physical human-robot interaction: Dependability, safety, and performance. In *Proc. 10th Intl. Workshop Advanced Motion Control*, pages 9–14, 2008.

[A3] M. G. Catalano, G. Grioli, F. Bonomo, R. Schiavi, and A. Bicchi. VSA-HD: From the enumeration analysis to the prototypical implementation. In *EEE/RSJ International Conference on Intelligent RObots and Systems*, pages 3676 – 3681, St. Louis MO USA, October 2010.

[A4] M. G. Catalano, G. Grioli, M. Garabini, F. Bonomo, M. Mancini, and A. Bicchi. VSA - CubeBot. a modular variable stiffness platform for multi degrees of freedom systems. In *2011 IEEE International Conference on Robotics and Automation*, Shangai, China, May 2011. Accepted.

[A5] A. Bicchi, M. G. Catalano, M. Garabini, and G. Grioli. Variable Plyability Actuator, October 2010. European Patent application EP10188315.5.

[A6] S. Alicino, M. G. Catalano, F. Bonomo, F. A. W. Belo, G. Grioli, R. Schiavi, A. Fagiolini, and A. Bicchi. A rough-terrain, casting robot for the esa lunar robotics challenge. In *Proc. IEEE/RSJ International Conference on Intelligent RObots and Systems*, pages 3336–3342, St. Louis MO USA, October, 11 - 15 2009.

[A7] E .P. Scilingo, M. Bianchi, G. Grioli, and A. Bicchi. Rendering softness: Integration of kinaesthetic and cutaneous information in a haptic device. *Transactions on Haptics*, 3(2):109 – 118, 2010.

[A8] M. Bianchi, G. Grioli, E. P. Scilingo, M. Santello, and A. Bicchi. Validation of a virtual reality environment to study anticipatory modulation of digit forces and position. In *Eurohaptics 2010*, volume 6192/2010 of *Lecture Notes in Computer Science*, pages 136 – 143, Amsterdam (The Netherlands), July, 8 - 10 2010.

[A9] A. Balestrino, A. Caiti, E. Crisostomi, and G. Grioli. A generalised entropy of curves: An approach to the analysis of dy-

BIBLIOGRAPHY

namical systems. In *Decision and Control, 2008. CDC 2008. 47th IEEE Conference on*, pages 1157–1162. IEEE, 2008.

[A10] Giorgio Grioli and Antonio Bicchi. A non-invasive real-time method for measuring variable stiffness. In *Proceedings of Robotics: Science and Systems*, Zaragoza, Spain, June 2010.

[A11] G. Grioli and A. Bicchi. A real-time parametric stiffness observer for VSA devices. In *2011 IEEE International Conference on Robotics and Automation*, Shangai, China, May 2011. Accepted.

[A12] A. Serio, G. Grioli, I. Sardellitti, N. G. Tsagarakis, and A. Bicchi. A decoupled impedance observer for a variable stiffness robot. In *2011 IEEE International Conference on Robotics and Automation*, Shangai, China, May 2011. Accepted.

Web sites

[W13] PHRIENDS: Phisical Human Robot Interaction depENDability and Safety. `www.phriends.eu`.

[W14] VIACTORS: Variable Impedance ACTuation systems embodying advanced interaction behaviORS. `www.viactors.eu`.

[W15] Model 8770A data sheet. `www.kistler.com`.

Miscellaneous

[16] N. Hogan. Impedance Control: An Approach to Manipulation: Part I II and III. *Journal of dynamic systems, measurement, and control*, 107:17, 1985.

[17] A. Albu-Schaeffer, C. Ott, and G. Hirzinger. A unified passivity-based control framework for position, torque and impedance control of flexible joint robots. *The International Journal of Robotics Research*, 26(1):23, 2007.

[18] A. Bicchi and G. Tonietti. Fast and soft-arm tactics. *IEEE Robotics and Automation Magazine*, 11(2):22–33, 2004.

[19] M. Uemura and S. Kawamura. Resonance-based motion control method for multi-joint robot through combining stiffness adaptation and iterative learning control. In *Proceedings of the 2009 IEEE international conference on Robotics and Automation*, pages 3398–3403. IEEE Press, 2009.

[20] S. Haddadin, T. Laue, U. Frese, S. Wolf, A. Albu-Schaeffer, and G. Hirzinger. Kick it like a safe robot: Requirements for 2050. *Robotics and Autonomous Systems: Special Issue on Humanoid Soccer Robots*, 57:761–775, 2008.

[21] G.A. Pratt and M.M. Williamson. Series elastic actuators. In *Proceedings of the IEEE/RSJ International Conference on*

BIBLIOGRAPHY

Intelligent Robots and Systems (IROS-95), volume 1, pages 399–406. IEEE, 1995.

[22] T. Morita and S. Sugano. Design and development of a new robot joint using a mechanical impedance adjuster. In *Robotics and Automation, 1995. Proceedings., 1995 IEEE International Conference on*, volume 3, pages 2469–2475. IEEE, 2002.

[23] A. Bicchi, G. Tonietti, M. Bavaro, and M. Piccigallo. Variable stiffness actuators for fast and safe motion control. *Robotics Research*, pages 527–536, 2005.

[24] R. Van Ham, B. Vanderborght, M. Van Damme, B. Verrelst, and D. Lefeber. MACCEPA, the mechanically adjustable compliance and controllable equilibrium position actuator: Design and implementation in a biped robot. *Robotics and Autonomous Systems*, 55(10):761–768, 2007.

[25] R. Van Ham, T.G. Sugar, B. Vanderborght, K.W. Hollander, and D. Lefeber. Review of actuators with passive adjustable compliance/controllable stiffness for robotic applications. *IEEE Robotics & Automation Magazine*, 1070(9932/09):81, 2009.

[26] M. Laffranchi, N.G. Tsagarakis and D.G. Caldwell *A variable physical damping actuator (VPDA) for compliant robotic joints*, 2010. In *Proc. IEEE Int. Conf. on Robotics and Automation*, pages 1668 – 1674, 2010.

[27] T. Takaki and T. Omata. Load-sensitive continuously variable transmission for powerful and inexpensive robot hands. In *Ro-*

botics and Automation, 2004. TExCRA'04. First IEEE Techni-cal Exhibition Based Conference on, pages 45–46. IEEE, 2004.

[28] R. Hooke and J. Yonge. *Lectures de Potentia Restitutiva, Or of Spring Explaining the Power of Springing Bodies...* Printed for John Martyn, 1678.

[29] S.I. Newton and N.W. Chittenden. *Newton's Principia: The mathematical principles of natural philosophy.* D. Adee, 1848.

[30] ISO VIM. International vocabulary of basic and general terms in metrology (VIM). *International Organization*, 2004:09–14, 2004.

[31] H. P. Olesen and R. B. Randall. A guide to mechanical im-pedance and structural response techniques. Technical report, Bruel & Kjaer, 1977.

[32] A.M. Wiggins. Mechanical Impedance Measuring Device, Au-gust 1944. US Patent 2,355,194.

[33] W.R. Koch. Method of and Means for Measuring Mechanical Impedance, February 1946. US Patent 2,394,455.

[34] R. Skalak and S. Chien. *Handbook of bioengineering.* McGraw-Hill New York, 1987.

[35] D.A. Winter. *Biomechanics and motor control of human move-ment.* John Wiley & Sons Inc, 2009.

[36] E. Burdet, R. Osu, D.W. Franklin, T. Yoshioka, T.E. Milner, and M. Kawato. A method for measuring endpoint stiffness

BIBLIOGRAPHY

during multi-joint arm movements. *Journal of biomechanics*, 33(12):1705–1709, 2000.

[37] C.W. De Silva and J.H. Gu. On-line sensing and modeling of mechanical impedance in robotic food processing. In *Systems, Man and Cybernetics, 1995. Intelligent Systems for the 21st Century., IEEE International Conference on*, volume 2, pages 1693–1698. IEEE, 1995.

[38] R.E. Kalman et al. A new approach to linear filtering and prediction problems. *Journal of basic Engineering*, 82(1):35–45, 1960.

[39] N. Diolaiti, C. Melchiorri, and S. Stramigioli. Contact impedance estimation for robotic systems. *Robotics, IEEE Transactions on*, 21(5):925–935, 2005.

[40] K.H. Hunt and F.R.E. Crossley. Coefficient of restitution interpreted as damping in vibroimpact. *Journal of Applied Mechanics*, 42:440, 1975.

[41] D. Erickson, M. Weber, and I. Sharf. Contact stiffness and damping estimation for robotic systems. *The International Journal of Robotics Research*, 22(1):41, 2003.

[42] F. Coutinho and R. Cortesao. System stiffness estimation with the candidate observers algorithm. In *Control & Automation (MED), 2010 18th Mediterranean Conference on*, pages 796–801. IEEE, 2010.

[43] K. Hashimoto, T. Kureha, Y. Nishimura, K. Okumura, and S. Muraoka. Measurement of mechanical impedance using quartz resonator force sensor during the process of grasping. In *SICE 2004 Annual Conference*, volume 1, pages 722–726. IEEE, 2004.

[44] D. Verscheure, I. Sharf, H. Bruyninckx, J. Swevers, and J. De Schutter. Identification of contact dynamics parameters for stiff robotic payloads. *Robotics, IEEE Transactions on*, 25(2):240–252, 2009.

[45] N. Hogan. Adaptive control of mechanical impedance by coactivation of antagonist muscles. *IEEE transactions on automatic control*, 29(8):681–690, 1984.

[46] A.G. Feldman. Functional tuning of the nervous system with control of movement or maintenance of a steady posture. II. Controllable parameters of the muscle. *Biophysics*, 11(3):565–578, 1966.

[47] S. Sastry and M. Bodson. *Adaptive control: stability, convergence, and robustness*. Prentice-Hall, 1989.

[48] L. Ljung. *System identification: theory for the user*, volume 280. Prentice-Hall NJ, 1987.

[49] A. Jafari, N.G. Tsagarakis, B. Vanderborght, and D.G. Caldwell. A novel actuator with adjustable stiffness (AwAS). In *Intelligent Robots and Systems (IROS), 2010 IEEE/RSJ International Conference on*, pages 4201–4206. IEEE, 2010.